QUATERNARY SCIENCE REVIEWS

The International Multidisciplinary Research and Review Journal

Volume 26 Nos 19–21 October 2007 ISSN 0277-3791

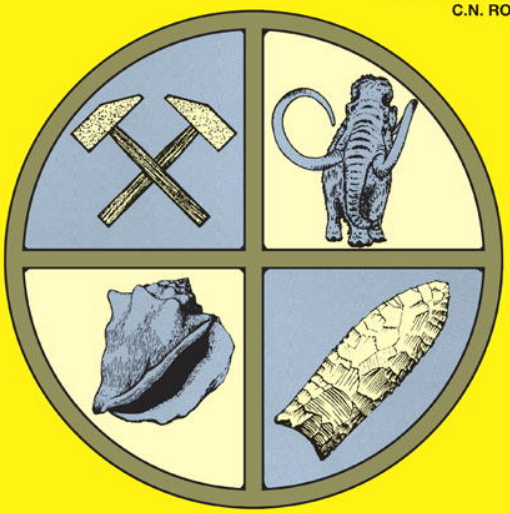

ELSEVIER

Quaternary Science Reviews 26 (2007) 2598–2616

QSR

The timing of linear dune activity in the Strzelecki and Tirari Deserts, Australia

Kathryn E. Fitzsimmons[a,b,*], Edward J. Rhodes[b,c,d], John W. Magee[a,b], Timothy T. Barrows[e]

[a]*Department of Earth and Marine Sciences, The Australian National University, Canberra, ACT 0200, Australia*
[b]*Cooperative Research Centre for Landscape Environments and Mineral Exploration (CRC LEME), The Australian National University, Canberra, ACT 0200, Australia*
[c]*Research School of Earth Sciences, The Australian National University, Canberra, ACT 0200, Australia*
[d]*Research School of Pacific and Asian Studies, The Australian National University, Canberra, ACT 0200, Australia*
[e]*Department of Nuclear Physics, Research School of Physical Sciences and Engineering, The Australian National University, Canberra, ACT 0200, Australia*

Received 15 January 2007; received in revised form 28 May 2007; accepted 12 June 2007

Abstract

Linear dunes occupy more than one-third of the Australian continent, but the timing of their formation is poorly understood. In this study, we collected 82 samples from 26 sites across the Strzelecki and Tirari Deserts in the driest part of central Australia to provide an optically stimulated luminescence chronology for these dunefields. The dunes preserve up to four stratigraphic horizons, bounded by palaeosols, which represent evidence for multiple periods of reactivation punctuated by episodes of increased environmental stability. Dune activity took place in episodes around 73–66, 35–32, 22–18 and 14–10 ka. Intermittent partial mobilisation persisted at other times throughout the last 75 ka and dune activity appears to have intensified during the late Holocene. Dune construction occurred when sediment was available for aeolian transport; in the Strzelecki and Tirari Deserts, this coincided with cold, arid conditions during Marine Isotope Stage (MIS) 4, late MIS 3 and MIS 2, and the warm, dry climates of the late Pleistocene–Holocene transition period and late Holocene. Localised influxes of sediment on active floodplains and lake floors during the relatively more humid periods of MIS 5 also resulted in dune formation. The timing of widespread dune reactivation coincided with glaciation in southeastern Australia, along with cooler temperatures in the adjacent oceans and Antarctica.

1. Introduction

The Australian desert dunes, which cover more than one-third of the continent (Jennings, 1968; Wasson et al., 1988), are considered to have formed under more widespread arid conditions in the past (Bowler, 1976). Previous workers suggested that multiple periods of aridity were responsible for the formation of desert dunes and the development of the extensive Australian dunefield, expressed as dune sand layers bounded by palaeosols (e.g. Bowler, 1976; Lomax et al., 2003). Earlier studies of desert dune activity in Australia have tended to focus on local areas (e.g. Callen, 1984; English et al., 2001; Lomax et al., 2003; Hollands et al., 2006). As a consequence, the timing and duration of these arid periods over large scales is poorly understood.

Previously, dating of desert dunes was hindered by the lack of suitable techniques or material with which to determine age. Limited attempts were made to date dunes by radiocarbon using the minimal organic material within them (Wasson, 1983), and less successfully, using the carbonate rootlets of palaeosols (Callen et al., 1983; Callen, 1984). Radiocarbon dating of a bone fragment in the substrate underlying a dune in the Tirari Desert led to the suggestion that the Australian dunefields are Holocene in age (Wopfner and Twidale, 1988), although most other studies indicate otherwise. The advent of luminescence dating techniques, which measure the time elapsed since

*Corresponding author. Department of Earth and Marine Sciences, The Australian National University, Canberra, ACT 0200, Australia. Tel.: +61 2 6125 2059; fax: +61 2 6125 5544.
E-mail address: Kathryn.Fitzsimmons@anu.edu.au (K.E. Fitzsimmons).

0277-3791/$ - see front matter © 2007 Elsevier Ltd. All rights reserved.
doi:10.1016/j.quascirev.2007.06.010

sediment grains were last exposed to sunlight (Aitken, 1985; Aitken, 1998), allowed direct dating of dune activity. Thermoluminescence (TL) dating was applied to the Australian linear dunes by Gardner et al. (1987), Readhead (1988) and Nanson et al. (1992a, 1995); these studies extended the length of the geomorphic record and indicated that widespread aeolian activity took place across the continent during the late Pleistocene, both around and following the Last Glacial Maximum (LGM). Such work effectively refuted the argument for the Holocene formation of the dunefield.

More recently, optically stimulated luminescence (OSL) dating of quartz has become the method of choice for dating dune deposition (e.g. Stokes et al., 1998; Thomas et al., 2000; Twidale et al., 2001; Lomax et al., 2003; Hollands et al., 2006). OSL makes use of electron traps within crystals which are more easily and effectively bleached by sunlight than those used in TL. This makes OSL an ideal technique for aeolian quartz grains, which are assumed to have been exposed to significant amounts of sunlight during deposition (Aitken, 1998). Chronologies of desert dunes obtained by OSL have generally supported the radiocarbon and TL age estimates for peak dune activity and aridity around the LGM (e.g. English et al., 2001; Lomax et al., 2003; Hollands et al., 2006), but have also highlighted complexities in the timing of episodes of dune reactivation across the world (Munyikwa, 2005).

This paper presents the largest dataset yet obtained of OSL age estimates from the Australian desert dunefields, using samples from the Strzelecki and Tirari Deserts in central Australia. The aim is to assess the timing of dune reactivation, and to establish whether desert dunes across a large region of Australia were active during discrete phases. This study refines the late Quaternary history of aridity of central Australia, in the context of global scale climatic change.

2. Regional setting

This study focuses on the linear dunefields of the Strzelecki and Tirari Deserts, located towards the eastern margin of the large anti-clockwise dune whorl that characterises the Australian dunefields (Fig. 1). The two dunefields lie in the most arid part of the Australian continent. This region falls within the southern part of the internally draining Lake Eyre basin, with the catchments of numerous (currently ephemeral) channels draining into the terminal playas of Lake Eyre and the Frome-Gregory system. Cooper Creek flows southwestward through both the Strzelecki and Tirari Deserts towards Lake Eyre, and Warburton Creek drains to the southwest along the northern margin of the Tirari Desert.

Extensive linear dunefields have developed downwind from the terminal playas of the basin, and are mostly relict forms. Arid conditions responsible for linear dune formation across the world today have been used as analogues for climatic conditions prevailing during the formation of relict dunefields (e.g. Lancaster, 1981). Transverse dunes, including lunettes, palaeoshorelines and source-bordering dunes, occur in association with playas and palaeolake margins, ephemeral creeks and palaeochannels. Transverse dunes have been identified as sources of sediment for the linear dunes which have developed downwind from them (Twidale, 1972; Fitzsimmons et al., 2007). In some areas, transverse dunes have been sufficiently truncated by reworking so that only subdued low ridges remain, over which linear dunes have migrated.

The Strzelecki and Tirari Desert dunefields form part of the most variable section of the continental dune whorl. Linear dunes in the south near Lake Frome are oriented west–southwest to east–northeast, and rotate to a more north–south trend in the northern Strzelecki Desert. In the Tirari Desert further west, dune orientation is slightly to the west of north (Fig. 1). The orientation of the linear dunes has been inferred to reflect palaeowind direction, based on modern relationships between linear dunes and wind regime (Brookfield, 1970; Fryberger, 1979; Wasson et al., 1988). These orientations are oblique to the current sand-shifting wind regime (Sprigg, 1982). Linear dunes are thought to have formed broadly longitudinal to the resultant vector of the palaeowind regime (Tsoar et al., 2004). In some places, linear dunes occur in secondary orientations oblique to both the dominant dune trend and the present wind regime, either underlying the dominant dunes (Fig. 2A) or occurring as oblique truncated dunes converging with the dominant orientation (Fig. 2B). Localised areas of intersecting dune trends were also noted in the Simpson Desert to the northeast by Mabbutt (1968). The preservation of multiple dune orientations not only represents the reorientation of linear dunes, but also likely changes in wind regime over time.

At present, arid conditions prevail across the region. Annual rainfall is less than 150 mm (Gentilli, 1986) with a high inter-annual variability (Schwerdtfeger and Curran, 1996). The northern part of the Tirari Desert receives the lowest annual rainfall, below 120 mm yr^{-1}, and is the most arid part of the continent at present, while the northern Strzelecki Desert receives up to 200 mm yr^{-1} (Gentilli, 1986). Despite these differences in average annual rainfall, the high inter-annual rainfall variability ensures that arid conditions prevail across the entire region, with the level of modern dune activity consistent across both dunefields. Modern aeolian activity is restricted to dune crests and rare whole linear dunes; transverse and lunette dunes are presently inactive. The linear dunes are at least partially vegetated, and intermittent partial activity appears to be dependent on the variable and highly sensitive state of vegetation and cyanobacterial crust cover (Hesse and Simpson, 2006).

2.1. Sites

Five study areas in the Strzelecki and Tirari Deserts were chosen, and were designated northern, central and south-

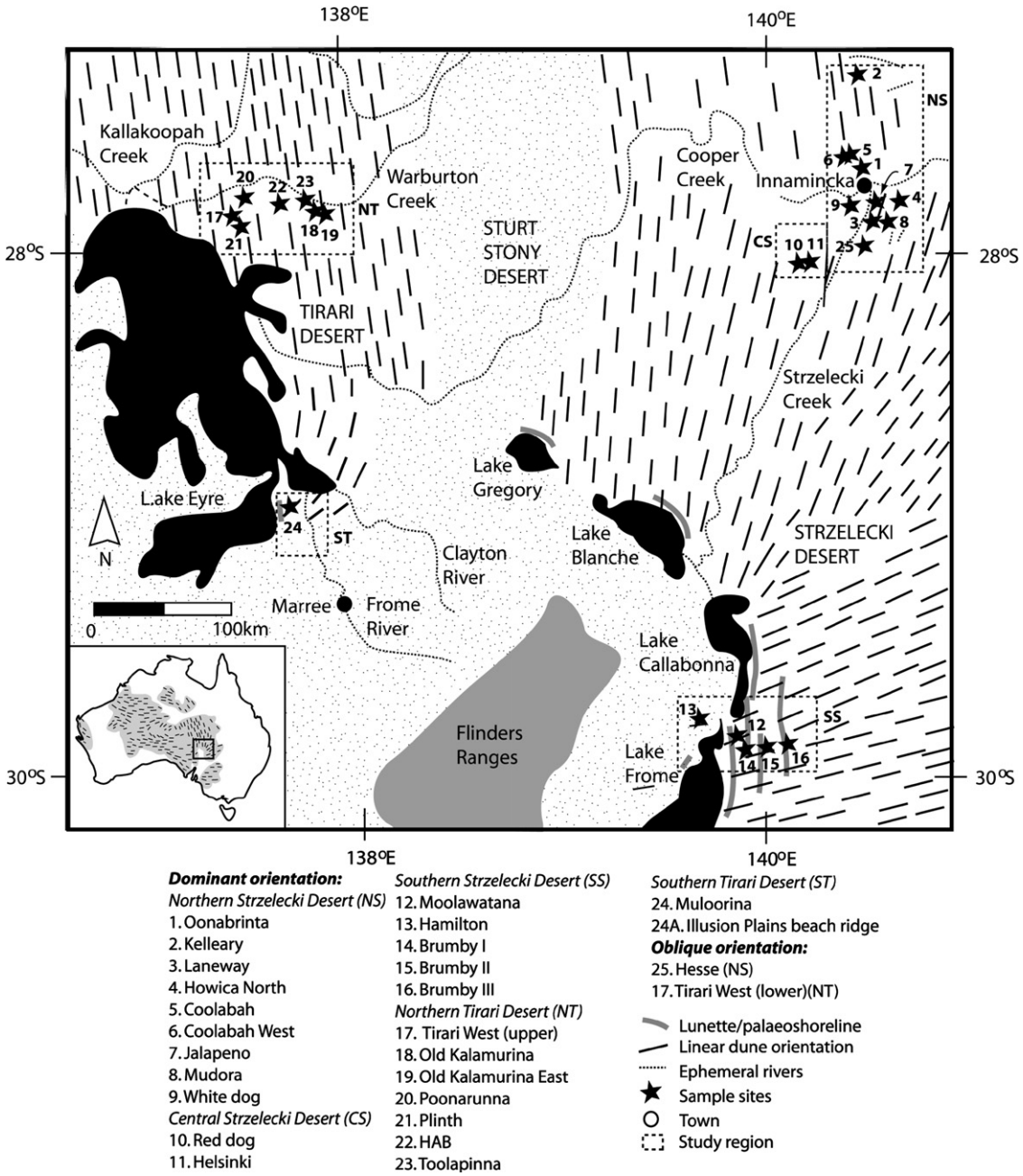

Fig. 1. Map of the Strzelecki and Tirari Deserts demonstrating the variable orientation of linear dunes across the study area, including the locations of the study regions and sample sites. Major lunettes, beach ridges and palaeoshorelines—including those discussed in this paper—are included in grey. Insert shows the Australian continental dune whorl (Wasson et al., 1988).

ern Strzelecki, and northern and southern Tirari Desert (Fig. 1). Linear dunes across these regions exhibit significant morphological variability, manifested by dune spacing, orientation and the density of junctions between dunes, and have developed on various substrates including floodplains, alluvial plains and stony plains (Brookfield, 1970; Wasson et al., 1988; Fitzsimmons, in press). Sampling sites were chosen from linear dunes with different characteristics across the dunefield to eliminate bias towards particular geomorphic contexts.

Fig. 2. Maps, cross sections and stratigraphy for sites described in detail in the text: (A) oblique and dominant linear dune orientations at the Tirari West (upper and lower) sites (TWU and TWL) in the northern Tirari Desert (image courtesy ASTER satellite imagery), (B) oblique truncated linear dunes converging with dunes of the dominant orientation at the Hesse (H) site in the northern Strzelecki Desert (image courtesy Shuttle DEM), (C) linear dunes overlying transverse dunes in the southern Strzelecki Desert, and (D) linear dunes extending downwind of old beach ridges at the Illusion Plains and Muloorina sites in the southern Tirari Desert. OSL sample depths are indicated; ages are shown in Fig. 3. Note the different scales for the maps and cross sections.

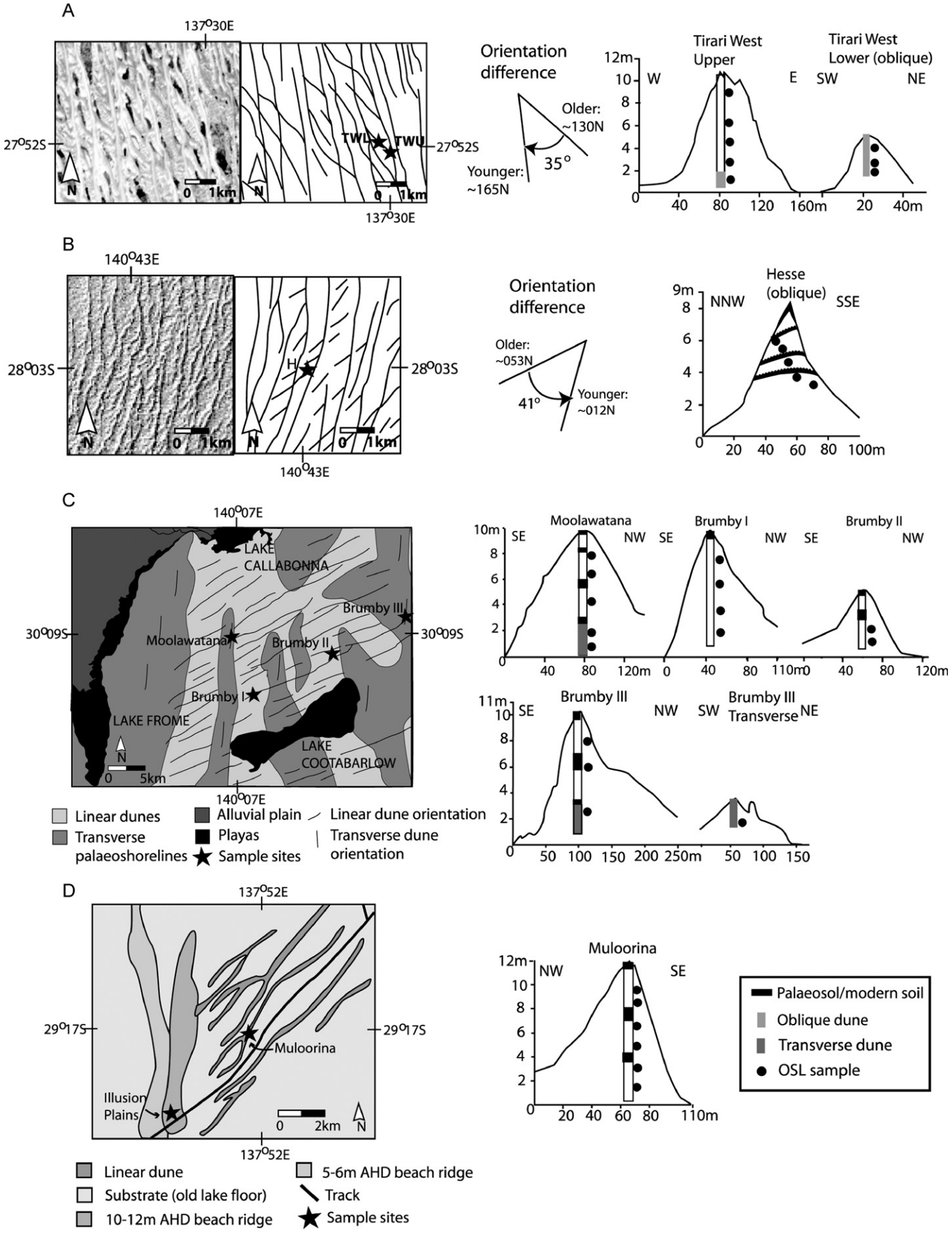

Table 1
Sample sites summary

Site name	Latitude	Longitude	Depositional environment	No. samples
Northern Strzelecki Desert				
Hesse	28°03′S	140°43′E	Obliquely oriented linear dune on floodplain sediment	5
Oonabrinta	27°40′S	140°43′E	Linear dune on stony plain, dominant orientation	2
Kelleary	27°02′S	140°44′E	Linear dune on alluvial sediment, dominant orientation	6
Laneway	27°54′S	140°44′E	Linear dune on floodplain sediment, dominant orientation	2
Howica North	27°47′S	140°54′E	Linear dune on alluvial sediment, dominant orientation	2
Coolabah	27°36′S	140°35′E	Linear dune on floodplain sediment, dominant orientation	1
Coolabah West	27°36′S	140°35′E	Linear dune on floodplain, dominant orientation	2
Jalapeno	27°49′S	140°45′E	Linear dune on stony plain, dominant orientation	2
Mudora	27°54′S	140°50′E	Linear dune on stony plain and floodplain, dominant orientation	4
White Dog	27°52′S	140°30′E	Linear dune on floodplain sediment, dominant orientation	3
Central Strzelecki Desert				
Red Dog	28°06′S	140°37′E	Large linear dune on floodplain, dominant orientation	3
Helsinki	28°08′S	140°40′E	Large linear dune on floodplain, dominant orientation	2
Southern Strzelecki Desert				
Moolawatana	30°09′S	140°06′E	Linear dune overlying transverse ridge, dominant orientation	5
Hamilton	30°06′S	139°59′E	Linear dune on alluvial sediment, dominant orientation	3
Brumby I	30°12′S	140°07′E	Linear dune, dominant orientation	4
Brumby II	30°10′S	140°11′E	Linear dune, dominant orientation	2
Brumby III	30°07′S	140°16′E	Linear dune overlying transverse ridge, dominant orientation	4 (including transverse ridge)
Northern Tirari Desert				
Tirari West (upper)	27°52′S	137°30′E	Linear dune on floodplain sediment, dominant orientation	5
Tirari West (lower)	27°52′S	137°30′E	Obliquely oriented linear dune on floodplain sediment	3
Old Kalamurina	27°57′S	138°03′E	Linear dune on alluvial sediment, dominant orientation	5
Old Kalamurina East	27°57′S	138°03′E	Linear dune on alluvial sediment, dominant orientation	1
Poonarunna	27°50′S	137°33′E	Linear dune on floodplain sediment, dominant orientation	4
Plinth	27°52′S	137°34′E	Linear dune, dominant orientation	1
HAB	27°54′S	137°49′E	Linear dune on alluvial sediment, dominant orientation	3
Toolapinna	27°52′S	137°54′E	Linear dune on alluvial sediment, dominant orientation	1
Southern Tirari Desert				
Muloorina	29°17′S	137°52′E	Linear dune on palaeolake floor, dominant orientation	6
Illusion Plains beach ridge	29°19′S	137°50′E	Aeolian unit overlying beach ridge crest	1

Twenty-six linear dunes were sampled across the five study regions (Fig. 1; Table 1). Of these, 24 sites are linear dunes aligned in the local dominant orientation, and two sites (Hesse and Tirari West (lower)) are oriented oblique to the main dunefield (Fig. 2A and B). At Kelleary and Mudora sites, samples were also taken from the underlying alluvial plain substrate. At two sites in the southern Strzelecki Desert, Moolawatana and Brumby III, linear dunes migrated over truncated transverse dunes (Fig. 2C). These transverse dunes were sampled by auger beneath the linear dune at Moolawatana, and both beneath the linear dune and separately at Brumby III. In the southern Tirari Desert, the Illusion Plains site represents an aeolian unit overlying a beach ridge which formed during previous high-lake stands of Lake Eyre (Magee and Miller, 1998; Magee et al., 2004) (Fig. 2D).

The dunes range from 3.5 to 14 m in height and from 40 to 250 m in width, and are at least partially vegetated, sometimes with active crests of loose sand. Spacing between the dune crests varies between 200 and 1000 m (Fitzsimmons, in press). Substrate material varies from old alluvial plains and floodplains to stony surfaces, and appears to influence the availability of sediment and dune spacing (Fitzsimmons, in press).

3. Methods

3.1. Field methods

OSL sampling was undertaken with the aim of sampling sediment which had not been reworked or bioturbated since deposition. Sediment within dune horizons probably represents the most recent activity within an episode of

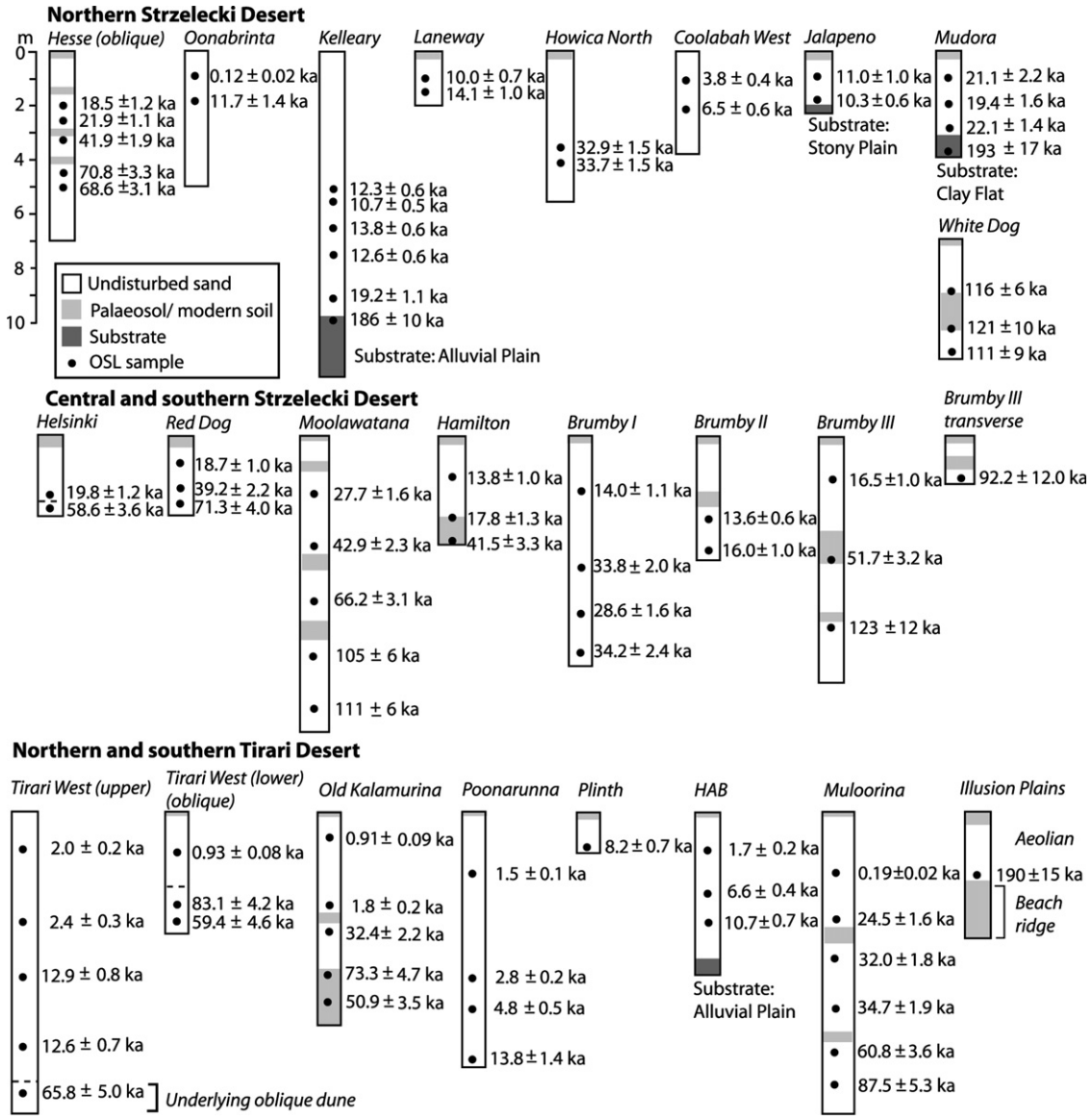

Fig. 3. Stratigraphy and OSL ages of individual sample sites. Note the uniform vertical scale.

dune reactivation. Sediment bioturbation due to mixing and exhumation can result in age underestimation, and was of greatest concern within palaeosols (e.g. Bateman et al., 2003). For this reason we sampled below visible zones of pedogenesis, identified by carbonate precipitation. Thin-section microscopy was later used to identify pedoturbated samples, as discussed in the results section.

At 11 sites, dune stratigraphy was exposed by creek incision, erosion on dune flanks or the creation of roads or tracks. These sites were sampled for OSL by driving stainless-steel tubes horizontally into cleaned, vertical surfaces. A microNomad sodium iodide portable gamma spectrometer, with a 3-inch crystal detector, was then inserted into the hole created by each tube. Gamma counting was undertaken for a minimum of half an hour.

Sites without stratigraphic exposure were sampled vertically by hand auger. The bucket sand auger extracted approximately 0.2 m sections of sediment, which were checked for evidence of soil development in the form of carbonate rhizomorphs, secondary gypsum and colour changes. OSL samples were collected from sediment below zones of pedogenesis, by attaching stainless-steel tubes to the auger stem and hammering into the sediment. Prior to OSL sampling, the depth of the OSL sampler down the hole was verified with the logged depth, to ensure that material had not fallen down the hole while withdrawing the auger. The conventional auger head was then reattached to the auger, and the hole widened in order to continue the hole. In situ sodium iodide spectrometry could not be undertaken down auger holes. There is a risk of sample contamination due to sand falling into the hole during the augering process; great care was taken to minimise this effect by careful augering and continual depth verification.

At all sites, the stratigraphy was recorded (Fig. 3), with particular attention paid to the depth and development of palaeosols. Observations were supported by thin-section

microscopy of sediments from all samples to identify microscopic-scale evidence for pedogenic development.

3.2. OSL dating laboratory procedures

The samples were given laboratory codes according to the sequence of processing in the laboratory, of K0001–K0017, K0052–K0068 and K0470–K0517 (Table 2). Samples were opened and processed under low-intensity red and yellow-orange light. Only the sediment in the central section of the tubes was processed for dating, to minimise the risk of potential exposure to light during collection and contamination due to the augering process. In situ moisture content was calculated by weighing the raw and oven-dried weight of material from the ends of the tubes.

Samples were treated to isolate quartz from other minerals in the sediment in order to obtain a pure quartz OSL signal. In the first step, dilute hydrochloric acid (HCl) was used to remove carbonates (e.g. Huntley et al., 1993). The modal grain size fractions were then isolated by sieving. Grains were etched by immersion in a solution of 40% hydrofluoric acid for 100 min to remove feldspars and the outer rinds of quartz exposed to alpha radiation, then rinsed in HCl and dried. Etching was followed by density separation using sodium polytungstate solution of 2.68 g cm^{-3} to remove heavy minerals (Rhodes, 1988), after which the clean quartz grains were re-sieved and mounted onto the central 3 of 10 mm diameter stainless-steel discs using silicone oil.

The effectiveness of chemical feldspar removal during etching was tested by analysing three etched samples for concentrations of three of the principle elements of feldspar, aluminium, calcium and potassium, using inductively coupled plasma mass spectrometry (ICPMS). The samples selected for analysis contained pre-etch feldspar proportions of 2.6–6.4%, determined from X-ray diffractometry. Feldspar content in the etched samples was reduced by an order of magnitude, indicating removal of the majority of feldspar. The infrared stimulated luminescence (IRSL) included as part of the SAR protocol prior to measuring the OSL signal yielded negligible IRSL signals, suggesting that very little feldspar remained in the samples.

3.3. Equivalent dose estimation

Equivalent dose (D_e) measurements were undertaken using automated Risø TL-DA-12 and TL-DA-15 readers. Light stimulation was provided by clusters of blue light-emitting diodes and a green filtered 150 W Halogen lamp (Bøtter-Jensen et al., 1999; Bøtter-Jensen et al., 2000), with the luminescence signal detected by EMI 9235QA photomultiplier tubes with coated Hoya U-340 filters (Bøtter-Jensen, 1997). Irradiation was undertaken using calibrated ^{90}Sr/^{90}Y beta sources (Bøtter-Jensen et al., 2000).

The single-aliquot regenerative-dose protocol (SAR) of Murray and Wintle (2000, 2003) was used to estimate the D_e of each sample. Fifteen aliquots were prepared, each consisting of approximately 200–300 grains, three of which were used to assess luminescence characteristics and determine the appropriate dose range for each sample. D_e determination was based on 12 aliquots, using a preheat of 10 s at 260 °C before OSL measurement of the natural dose and four regenerated dose points, and a 10 s treatment at 220 °C before sensitivity correction OSL measurements (Murray and Wintle, 2000). Preheat temperatures were based on the results of preheat plateau tests of comparable sediments from the dunefields, which indicated palaeodose stability with preheating (Rhodes, unpublished data). Potential thermal transfer was identified by the signal arising from a zero dose step. Thermal transfer was generally $<2\%$ and therefore negligible for the purposes of D_e determination, though several young samples from the Tirari Desert (K0488, K0489, K0493, K0501, K0502) exhibited thermal transfer values up to 8%, possibly related to incomplete bleaching or the relatively high preheat temperatures used. Following Murray and Wintle (2000, 2003), the sensitivity changes induced within the SAR protocol were assessed by calculating recycling values for each sample. Recycling values were all within 5% and were therefore judged acceptable.

A few samples included aliquots with D_e values clearly lying beyond the mean. Following numerical simulation of the effects of the incorporation of a small quantity of grains with different D_e values, for example owing to incomplete zeroing (Rhodes, 2007), aliquots lying beyond 3σ from the normal distribution peak were removed prior to D_e calculation using a weighted mean.

3.4. Dose rate determination

The concentrations of radioactive elements K, Th and U were measured using neutron activation analysis (NAA) for samples K0001–K0017 and K0052–K0068 at Becquerel Laboratories, Lucas Heights, New South Wales. For samples K0470–K0517, ICPMS was used to measure U and Th content, and inductively coupled plasma atomic emission spectrometry (ICPAES) for K content, at Genalysis Laboratories, Perth, Western Australia. Seventeen samples were measured using in situ sodium iodide spectrometry at the sample point, and 13 samples were analysed for radioactive element activities and uranium-series disequilibrium using high-resolution germanium gamma spectrometry (HRGS) (Table 2) (three samples were analysed using both gamma spectrometry techniques). These two techniques were used to calculate the gamma component of the dose rate for the relevant samples. Element concentrations derived from NAA, ICPMS and ICPAES were used to calculate the beta component only for those samples with gamma spectrometry data, and both the beta and gamma components where gamma spectrometry was not available. HRGS was also used to identify potential disequilibrium in the decay chains of uranium and thorium. For all samples analysed using HRGS except

Table 2
Equivalent dose (D_e), dose rate data and OSL age estimates for all samples, listed by region

Sample ID	Site	Depth (m)[a]	D_e (Gy)	Radionuclide concentrations			External γ dose rate (Gy/ka)	Cosmic ray dose rate (Gy/ka)[b]	Total dose rate (Gy/ka)	Age estimate (ka)
				K (%)	Th (ppm)	U (ppm)				
Northern Strzelecki Desert										
Oblique orientation										
K0010	Hesse	1.5	10.60±0.27	0.17±0.01[c]	1.90±0.10[c]	0.30±0.02[c]	0.20±0.00[e]	0.17±0.03	0.57±0.03	18.5±1.2
K0009		2.5	13.20±0.40	0.18±0.01[c]	2.03±0.10[c]	0.40±0.02[c]	0.23±0.00[d]	0.15±0.02	0.60±0.02	21.9±1.1
K0008		3.0	27.21±0.81	0.22±0.01[c]	2.24±0.11[c]	0.50±0.03[c]	0.24±0.00[e]	0.14±0.02	0.65±0.02	41.9±1.9
K0007		3.5	41.22±1.22	0.20±0.01[c]	2.29±0.12[c]	0.42±0.02[c]	0.21±0.00[e]	0.13±0.01	0.58±0.02	70.8±3.3
K0006		4	42.76±1.24	0.23±0.01[c]	2.41±0.12[c]	0.36±0.02[c]	0.24±0.01[d]	0.13±0.01	0.62±0.02	68.6±3.1
Dominant orientation										
K0052	Oonabrinta	1.5	0.06±0.01	0.16±0.01[c]	1.27±0.06[c]	0.25±0.04[c]	0.13±0.00[e]	0.17±0.03	0.47±0.03	0.12±0.02
K0053		0.75	7.07±0.33	0.20±0.01[c]	1.63±0.08[c]	0.42±0.02[c]	0.19±0.00[e]	0.19±0.06	0.60±0.07	11.7±1.4
K0054	Kelleary	5.1	6.84±0.22	0.23±0.01[c]	1.65±0.08[c]	0.41±0.02[c]	0.20±0.00[e]	0.11±0.01	0.56±0.02	12.1±0.6
K0055		6.2	9.16±0.29	0.44±0.02[c]	3.15±0.16[c]	0.49±0.03[c]	0.31±0.00[e]	0.10±0.01	0.85±0.03	10.7±0.5
K0056		5.8	6.90±0.21	0.12±0.01[c]	1.13±0.06[c]	0.31±0.02[c]	0.25±0.00[e]	0.10±0.01	0.50±0.01	13.8±0.6
K0057		6.5	9.59±0.24	0.37±0.02[c]	2.59±0.13[c]	0.42±0.02[c]	0.30±0.00[e]	0.10±0.01	0.76±0.03	12.6±0.5
K0058		7.8	18.14±0.67	0.52±0.03[c]	3.30±0.17[c]	0.72±0.04[c]	0.33±0.00[e]	0.08±0.01	0.94±0.04	19.2±1.1
K0059[1]		4.6	18.14±0.67	0.48±0.02[c]	3.03±0.15[c]	0.64±0.03[c]	0.34±0.00[e]	0.12±0.01	0.94±0.03	186±10
K0063	Laneway	1.2	6.90±0.20	0.21±0.01[c]	2.69±0.13[c]	0.56±0.03[c]	–	0.18±0.04	0.69±0.05	10.0±0.7
K0064		1.9	10.40±0.50	0.27±0.01[c]	2.74±0.14[c]	0.56±0.03[c]	–	0.16±0.02	0.74±0.04	14.1±1.0
K0065	Howica North	3.7	22.19±0.62	0.23±0.01[c]	2.85±0.14[c]	0.59±0.03[c]	0.25±0.00[e]	0.13±0.01	0.68±0.02	32.9±1.5
K0066		5.3	23.03±0.67	0.27±0.01[c]	2.63±0.13[c]	0.52±0.03[c]	0.26±0.00[e]	0.11±0.01	0.68±0.02	33.7±1.5
K0470	Coolabah	8.5	21.29±0.75	0.34±0.02[f]	2.10±0.11[f]	0.57±0.11[f]	–	0.08±0.01	0.67±0.04	32.0±2.2
K0477	Coolabah West	1.1	1.86±0.12	0.17±0.01[f]	1.25±0.06[f]	0.28±0.06[f]	–	0.18±0.02	0.49±0.05	3.8±0.4
K0478		2.1	3.28±0.21	0.19±0.01[f]	1.32±0.07[f]	0.35±0.07[f]	–	0.16±0.01	0.51±0.03	6.5±0.6
K0471	Jalapeno	1.2	6.20±0.26	0.20±0.01[f]	1.68±0.08[f]	0.36±0.07[f]	–	0.18±0.02	0.56±0.05	11.0±1.0
K0472		2.0	5.83±0.01	0.16±0.01[f]	2.10±0.11[f]	0.57±0.11[f]	0.18±0.00[d]	0.16±0.02	0.57±0.03	10.3±0.6
K0473	Mudora	1.2	11.02±0.58	0.17±0.01[f]	1.67±0.08[f]	0.30±0.06[f]	–	0.18±0.02	0.52±0.05	21.1±2.2
K0474		2.1	9.98±0.33	0.16±0.01[f]	1.43±0.07[f]	0.28±0.06[f]	0.18±0.00[d]	0.16±0.02	0.52±0.03	19.4±1.6
K0475		3.2	15.36±0.51	0.28±0.01[f]	2.91±0.15[f]	0.47±0.09[f]	–	0.14±0.01	0.70±0.04	22.1±1.4
K0476[2]		3.8	154.64±9.91	0.30±0.01[f]	3.27±0.16[f]	0.76±0.15[f]	–	0.13±0.01	0.80±0.05	193±17
K0479	White Dog	1.9	100.77±0.22	0.39±0.02[f]	2.46±0.12[f]	0.58±0.11[f]	0.30±0.00[d]	0.16±0.02	0.87±0.04	116±6
K0480		3.6	104.44±6.32	0.42±0.02[f]	2.62±0.13[f]	0.69±0.13[f]	–	0.13±0.01	0.86±0.05	121±10
K0481		4.3	106.88±6.58	0.48±0.02[f]	3.21±0.16[f]	0.77±0.03[f]	–	0.12±0.01	0.96±0.05	111±9
Central Strzelecki Desert										
Dominant orientation										
K0060	Red Dog	2.7	10.94±0.36	0.21±0.01[c]	2.01±0.10[c]	0.45±0.02[c]	–	0.15±0.02	0.59±0.03	18.7±1.1
K0061		3.4	21.98±0.74	0.20±0.01[c]	2.11±0.11[c]	0.41±0.02[c]	–	0.14±0.01	0.56±0.03	39.2±2.2
K0062		2.7	41.50±1.32	0.19±0.01[c]	2.00±0.10[c]	0.51±0.03[c]	–	0.15±0.02	0.58±0.03	71.3±4.0
K0068	Helsinki	2.2	13.21±0.54	0.23±0.01[c]	2.35±0.12[c]	0.50±0.03[c]	0.23±0.00[e]	0.16±0.02	0.67±0.03	19.8±1.2
K0067		2.7	36.52±1.69	0.22±0.01[c]	2.17±0.11[c]	0.36±0.02[c]	0.23±0.00[e]	0.15±0.02	0.62±0.02	58.6±3.5

Table 2 (*continued*)

Sample ID	Site	Depth (m)[a]	D_e (Gy)	Radionuclide concentrations			External γ dose rate (Gy/ka)	Cosmic ray dose rate (Gy/ka)[b]	Total dose rate (Gy/ka)	Age estimate (ka)
				K (%)	Th (ppm)	U (ppm)				
Southern Strzelecki Desert										
Linear dunes										
K0001	Moolawatana[3]	2.1	62.91±1.74	1.31±0.07[c]	8.45±0.42[c]	1.25±0.06[c]	–	0.16±0.02	2.27±0.11	27.7±1.6
K0002		4.1	106.26±3.21	1.24±0.06[c]	10.90±0.55[c]	1.85±0.09[c]	–	0.12±0.01	2.48±0.11	42.9±2.3
K0003		6.1	155.50±4.18	1.33±0.07[c]	10.30±0.52[c]	1.49±0.08[c]	0.89±0.01[d]	0.10±0.01	2.35±0.09	66.2±3.1
K0004[4]		8.2	266.23±9.61	1.35±0.07[c]	11.40±0.57[c]	1.67±0.08[c]	–	0.08±0.01	2.53±0.12	105±6
K0005[4]		10.3	299.21±9.21	1.27±0.06[c]	13.40±0.67[c]	2.21±0.11[c]	–	0.07±0.01	2.70±0.12	110±6.0
K0508	Hamilton	1.6	37.92±1.68	1.53±0.08[f]	10.42±0.52[f]	1.91±0.37[f]	–	0.17±0.02	2.75±0.16	13.8±1.0
K0509		3.2	53.01±2.47	1.56±0.08[f]	13.00±0.65[f]	2.15±0.42[f]	–	0.14±0.01	2.98±0.17	17.7±1.3
K0510		4.2	96.09±5.37	1.40±0.07[f]	7.58±0.38[f]	1.59±0.31[f]	–	0.12±0.01	2.32±0.13	41.5±3.3
K0514	Brumby I	2.1	27.68±1.51	1.03±0.05[f]	7.78±0.39[f]	1.43±0.28[f]	–	0.16±0.01	1.99±0.11	14.0±1.1
K0515		5.0	52.25±1.47	1.11±0.06[f]	6.41±0.32[f]	1.12±0.22[f]	–	0.11±0.01	1.84±0.10	33.8±2.0
K0516		6.6	60.56±0.62	1.04±0.05[f]	7.81±0.39[f]	1.59±0.31[f]	0.91±0.011[d]	0.09±0.01	2.12±0.08	28.6±1.6
K0517		8.2	70.11±2.93	1.10±0.06[f]	8.29±0.41[f]	1.64±0.32[f]	–	0.08±0.01	2.05±0.12	34.2±2.4
K0512	Brumby II	3.0	26.96±6.08	1.01±0.05[f]	6.93±0.35[f]	1.15±0.22[f]	0.83±0.011[d]	0.14±0.02	1.99±0.08	13.6±0.6
K0513		4.2	30.75±1.03	1.04±0.05[f]	7.53±0.38[f]	1.36±0.27[f]	–	0.12±0.01	1.92±0.11	16.0±1.0
K0505	Brumby III	1.7	28.49±2.74	0.87±0.04[f]	6.82±0.34[f]	1.20±0.24[f]	–	0.17±0.02	1.72±0.10	16.5±1.8
K0506		4.6	91.62±0.24	0.84±0.04[f]	7.18±0.36[f]	1.16±0.23[f]	0.75±0.01[d]	0.12±0.01	1.77±0.07	51.7±3.2
K0507[4]		7.1	214.22±15.84	0.85±0.04[f]	7.53±0.38[f]	1.51±0.30[f]	–	0.09±0.01	1.75±0.10	123±12
Transverse dune ridge										
K0511	Brumby III transverse	1.7	168.72±0.67	0.87±0.04[f]	6.6±0.33[f]	1.39±0.27[f]	0.73±0.01[d]	0.17±0.03	1.83±0.07	92.2±11.9
Northern Tirari Desert										
Oblique orientation										
K0493	Tirari West (Lower)	1.6	0.89±0.05	0.49±0.02[f]	2.74±0.14[f]	0.61±0.12[f]	–	0.17±0.03	0.96±0.06	0.9±0.1
K0494		3.5	71.42±0.21	0.44±0.02[f]	1.81±0.09[f]	0.61±0.12[f]	0.30±0.00[d]	0.13±0.01	0.86±0.04	83.1±4.2
K0495		4.2	55.43±2.14	0.46±0.02[f]	2.01±0.10[f]	1.07±0.21[f]	–	0.12±0.01	0.93±0.06	59.4±9.6
Dominant orientation										
K0488	Tirari West (Upper)	1.6	1.69±0.17	0.50±0.02[f]	1.92±0.10[f]	0.49±0.10[f]	–	0.17±0.02	0.88±0.05	2.0±0.2
K0489		4.2	2.10±0.20	0.51±0.03[f]	1.91±0.10[f]	0.49±0.10[f]	–	0.12±0.01	0.85±0.05	2.4±0.3
K0490		6.2	9.88±0.27	0.47±0.02[f]	1.75±0.09[f]	0.46±0.09[f]	–	0.10±0.01	0.76±0.04	12.9±0.8
K0491		8.6	9.64±0.29	0.44±0.02[f]	1.86±0.09[f]	0.51±0.10[f]	0.27±0.00[d]	0.08±0.01	0.76±0.03	12.6±0.7
K0492[5]		10.2	67.09±1.63	0.52±0.03[f]	2.42±0.12[f]	1.32±0.26[f]	–	0.07±0.01	1.02±0.07	65.8±5.0
K0482	Old Kalamurina	1.1	0.51±0.02	0.23±0.01[f]	1.34±0.07[f]	0.32±0.06[f]	–	0.18±0.02	0.56±0.05	0.9±0.1
K0483		3.7	1.35±0.10	0.37±0.02[f]	2.33±0.12[f]	0.46±0.09[f]	–	0.13±0.01	0.74±0.04	1.8±0.2
K0484		4.7	22.53±0.94	0.37±0.02[f]	1.96±0.10[f]	0.45±0.09[f]	–	0.12±0.01	0.70±0.04	32.4±2.2
K0485		6.3	57.68±1.78	0.45±0.02[f]	2.06±0.10[f]	0.55±0.11[f]	–	0.10±0.01	0.79±0.04	73.3±4.7
K0486		7.4	40.07±1.35	0.42±0.02[f]	2.06±0.10[f]	0.72±0.14[f]	–	0.09±0.01	0.79±0.05	50.9±3.5
K0487	Old Kalamurina East	1.4	6.65±0.29	0.32±0.02[f]	1.61±0.08[f]	0.39±0.08[f]	–	0.17±0.02	0.67±0.05	9.8±0.8

K0496	Poonarunna	2.4	1.03±0.04	0.34±0.02[f]	1.78±0.09[f]	0.46±0.09[f]	–	0.15±0.01	0.70±0.04	1.5±0.1
K0497		6.2	2.18±0.1	0.44±0.02[f]	2.19±0.11[f]	0.51±0.10[f]	–	0.10±0.01	0.78±0.04	2.8±0.2
K0498		7.3	5.16±0.49	0.60±0.03[f]	3.47±0.17[f]	0.84±0.16[f]	–	0.09±0.01	1.08±0.06	4.8±0.5
K0499		9.2	12.25±1.03	0.48±0.02[f]	2.96±0.15[f]	0.73±0.14[f]	–	0.07±0.01	0.89±0.05	13.8±1.4
K0500	Plinth	1.4	7.75±0.44	0.50±0.03[f]	2.40±0.12[f]	0.59±0.12[f]	–	0.17±0.02	0.95±0.06	8.2±0.7
K0501	HAB[6]	1.7	1.32±0.14	0.41±0.02[f]	1.77±0.09[f]	0.46±0.09[f]	–	0.17±0.02	0.78±0.05	1.7±0.2
K0502		3.1	5.30±0.13	0.40±0.02[f]	2.34±0.12[f]	0.58±0.11[f]	–	0.14±0.01	0.80±0.05	6.6±0.4
K0503		4.1	7.74±0.30	0.39±0.02[f]	1.80±0.09[f]	0.46±0.09[f]	–	0.12±0.01	0.72±0.04	10.7±0.7
K0011	Toolapinna	2.0	27.57±0.74	0.45±0.02[e]	2.28±0.11[e]	0.46±0.02[e]	–	0.16±0.02	0.86±0.04	32.2±1.9
Southern Tirari Desert										
Linear dune										
K0017	Muloorina	2.0	0.10±0.01	0.18±0.01[e]	1.71±0.09[e]	0.40±0.02[e]	–	0.16±0.02	0.54±0.03	0.19±0.02
K0012		4.0	18.61±0.88	0.33±0.02[e]	2.60±0.13[e]	0.62±0.03[e]	–	0.13±0.01	0.76±0.03	24.5±1.6
K0014		5.5	25.33±0.95	0.36±0.02[e]	2.56±0.13[e]	0.74±0.04[e]	–	0.11±0.01	0.79±0.03	32.0±1.8
K0015		7.0	28.20±1.06	0.44±0.02[e]	2.66±0.13[e]	0.69±0.35[e]	0.27±0.00[d]	0.09±0.01	0.81±0.03	34.7±1.9
K0016		8.5	47.59±1.95	0.35±0.02[e]	2.30±0.12[e]	0.91±0.05[e]	–	0.08±0.01	0.78±0.03	60.8±3.6
K0013		10.0	56.78±2.13	0.36±0.02[e]	2.25±0.11[e]	0.37±0.02[e]	–	0.07±0.01	0.65±0.03	87.5±5.3
Aeolian cap on beach ridge										
K0504	Illusion Plains	2.5	176.14±7.41	0.35±0.02[f]	2.68±0.13[f]	1.14±0.22[f]	–	0.15±0.02	0.93±0.06	190±15

Ages from individual sites are presented in stratigraphic order.

[a]Depth was measured from the dune surface to the sample point. In some cases, samples were taken from the dune flanks rather than the crest.

[b]Cosmic ray dose rates were calculated following Prescott and Hutton (1994) according to current depth from surface, based upon values for sediment density, altitude, latitude and longitude.

[c]Measured by INAA (Becquerel Laboratories, ANSTO, Australia).

[d]Derived from HRGS (CSIRO, Canberra, Australia).

[e]Derived from in situ portable sodium iodide gamma spectrometry.

[f]Measured by ICPMS (Genalysis Laboratories, Perth, Australia).

[1]Sample K0059 taken from alluvial substrate excavated beneath dune flank at Kelleary site.

[2]Sample K0476 taken from clay flat substrate augered beneath dune crest at Mudora site.

[3]Samples K0001–K0005 published previously in Fitzsimmons et al. (2007), with the exception of K0003, calculated here using high-resolution germanium gamma spectrometry and INAA data.

[4]Samples K0004, K0005 and K0507 taken from transverse dune ridges underlying the Moolawatana (K0004, K0005) and Brumby III (K0507) linear dunes. Sample K0507 corresponds both stratigraphically and geomorphically to sample K0511.

[5]Sample K0492 taken from obliquely oriented linear dune ridge underlying the Tirari West linear dune, and corresponds both stratigraphically and geomorphically to samples K0494 and K0495 (Tirari West (Lower)).

[6]Samples K0501–K0503 published previously in Fitzsimmons and Telfer (in press).

Table 3
Activities of members of the ^{238}U and ^{232}Th decay chains, measured by HRGS

Sample	^{238}U (Bq/kg)	^{226}Ra (Bq/kg)	^{210}Pb (Bq/kg)	^{228}Ra (Bq/kg)	^{228}Th (Bq/kg)
K0003	21.84±2.85	19.62±0.44	19.43±3.69	38.53±1.04	38.73±0.89
K0006	7.30±0.95	7.64±0.17	7.73±1.18	9.89±0.37	9.56±0.27
K0009	6.71±0.71	7.72±0.14	7.67±0.83	9.74±0.26	9.40±0.22
K0015	7.91±0.75	8.47±0.15	9.69±0.87	8.88±0.26	9.37±0.23
K0056	7.21±1.16	6.82±0.18	9.39±1.45	3.52±0.31	6.14±0.24
K0472	6.24±0.65	5.93±0.12	6.11±0.74	7.38±0.23	7.60±0.19
K0474	4.87±1.08	6.12±0.16	6.05±1.34	7.46±0.36	7.31±0.24
K0479	8.39±0.62	8.89±0.14	9.77±0.71	11.05±0.24	10.72±0.22
K0491	7.14±0.71	7.96±0.14	6.49±0.87	8.63±0.25	8.36±0.21
K0494	8.09±0.74	10.02±0.16	10.12±0.91	8.65±0.24	8.50±0.21
K0506	16.65±1.04	17.16±0.25	17.65±1.27	33.68±0.54	33.88±0.59
K0511	16.40±1.41	17.54±0.29	17.28±1.69	31.46±0.62	31.16±0.60
K0512	18.90±1.70	19.06±0.34	20.22±2.19	35.62±0.81	36.46±0.73
K0516	17.19±1.50	19.88±0.32	21.07±1.90	41.44±0.75	40.40±0.75

K0056, both the uranium and thorium series decay chains appear to be in secular equilibrium within measurement error (Table 3). Sample K0056 is in disequilibrium within the thorium series decay chain; however, the short half lives of its daughter isotopes mean that disequilibrium is relatively unimportant in these sediments, which are considerably older than the thorium daughter half lives (Olley et al., 1996). Since the samples analysed for HRGS were chosen to be representative of the sample suite, the results suggest that the other samples are also currently in secular equilibrium.

Dose rates were calculated from radionuclide concentrations and activities using the conversion factors of Adamiec and Aitken (1998). ICPMS measurements showed a systematic underestimation of uranium concentration relative to the other techniques. This was quantified according to the average deviation from the dose rates calculated from the other dosimetry techniques and corrected for those samples for which ICPMS had been undertaken. The modern mean water content of the samples (5±3%) was assumed to represent the long-term and spatial average, and was incorporated into dose rate calculations to correct for the attenuation of radiation by moisture. Beta dose attenuation was estimated using the values of Mejdahl (1979). Cosmic-ray dose rates were determined from the sample depths and uniform values for sediment density and site altitude, latitude and longitude, following Prescott and Hutton (1994).

4. Results

The age estimates and data used for age calculation are presented in Table 2. The OSL behaviour of the samples indicates that the central Australian dune sands are well suited to OSL dating techniques, with samples exhibiting intense initial OSL signals with rapid decay. IRSL signals and thermal transfer are generally low, and aliquots demonstrate good recycling values and dose recovery, reinforcing the suitability of the samples to the SAR protocol. Samples from the southern Strzelecki Desert exhibit high dose rates (Table 2), most likely related to the relatively high proportions of clay within the sediment, derived from radioactive basement rocks in the Flinders Ranges to the west (Pell et al., 2000). However, none of the samples had OSL data approaching saturation.

The ages from Moolawatana and HAB have been discussed previously at the local scale in Fitzsimmons et al. (2007) and Fitzsimmons and Telfer (in press), respectively.

Fig. 3 shows the position of palaeosols within the stratigraphy of individual dunes, giving some indication of the possible timing of pedogenesis and hiatuses in aeolian activity. However, the exact timing of palaeosol formation is not constrained by these OSL age estimates.

The majority of the OSL ages are consistent with the stratigraphy at the sites (Fig. 3). Four samples (K0485, K0486, K0494, K0495) were excluded from the regional interpretation due to age inversion, interpreted to have resulted from contamination during sampling. A further five samples (K0480, K0481, K0506, K0509, K0510) were identified as pedoturbated from thin-section microscopy of the sediments following fieldwork. Evidence of pedogenesis was interpreted from the presence of intact grain coatings in all of these samples as a result of clay illuviation (Fitzsimmons et al., 2007), and pedogenic carbonates in K0506, K0509 and K0510.

4.1. Linear dune age clustering

An age-ranked chronology and relative probability plot of the linear dunes is presented in Fig. 4. The relative probability plot (Fig. 4B) represents the normalised sum of the probability distributions of individual ages, and is included for visual comparison of age groupings. Clusters of similar ages form peaks, and the height of the peaks is a function of the number of ages in the cluster and the fractional error of the ages. Therefore, young peaks will be

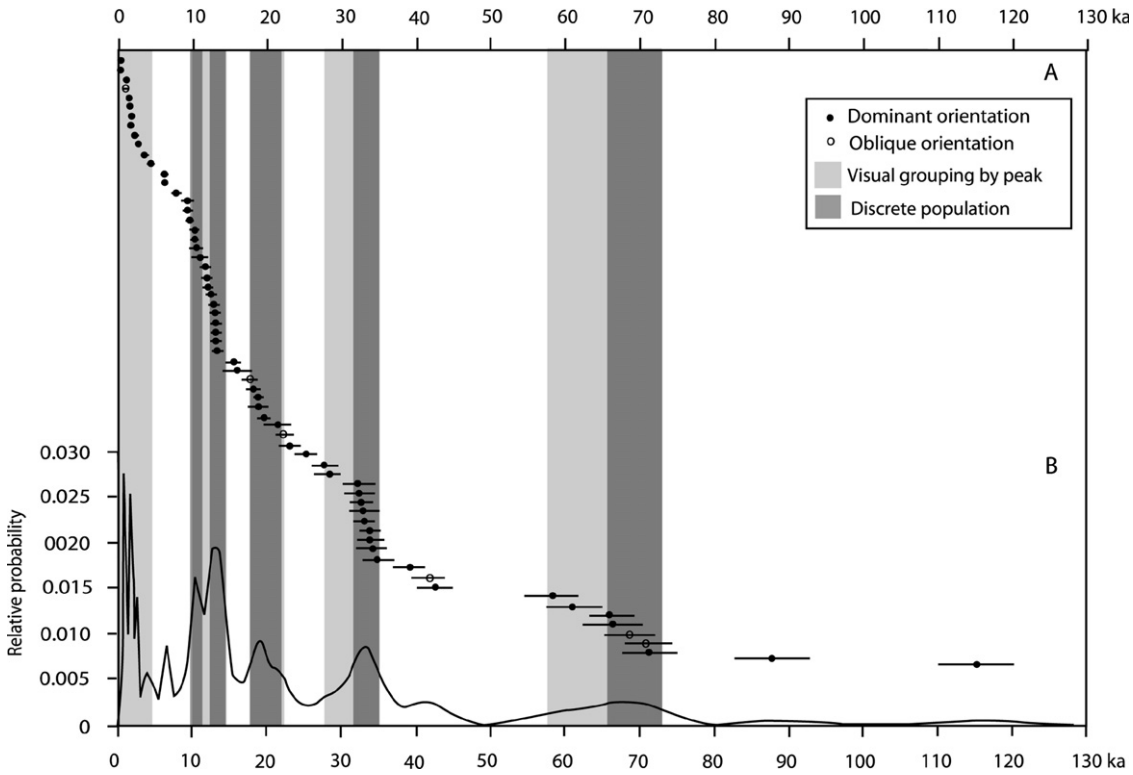

Fig. 4. (A) Age-ranked plot of age estimates, and (B) relative probability plot of ages, from linear dunes in the Strzelecki and Tirari Deserts. Age groupings for dune activity are highlighted in grey.

higher than older peaks, despite being composed of the same number of ages with the same fractional error.

Five distinct peaks were identified at approximately 73–59, 35–32, 22–18, 14–10 and 4–0 ka. Reduced χ^2-tests were undertaken on the ages within each of these peaks to determine whether they each represent a single age event. Within 73.3–58.6 ka, the nine ages might constitute a single population where the dispersion is consistent with the ascribed errors ($\chi^2/\nu = 2.22$, age of 66.1 ± 5.4 ka). However, the six ages from 73.3 to 65.8 are much more likely to represent a single event ($\chi^2/\nu = 0.55$, age of 69.3 ± 3.0 a). From 34.7–32.0 ka, eight ages are very likely to represent a single event ($\chi^2/\nu = 0.27$, age of 33.1 ± 1.0 ka). The 9 ages from 22.1–17.8 ka are likely to represent a single event ($\chi^2/\nu = 1.49$, age of 19.8 ± 1.5 ka). From 14.1–10.0 ka, there are two distinct peaks representing two populations in the 16 ages from 11.7–10.0 ka ($\chi^2/\nu = 0.45$, age of 10.7 ± 0.5 ka) and 14.1–12.1 ka ($\chi^2/\nu = 1.00$, age of 13.3 ± 0.6 ka). Ages falling within the period 3.8–0 ka, which appear as several peaks on the relative probability plot, do not fit a single population, although it is clear that dune activity appears to increase in frequency around this time. The visual age groupings and statistical populations are highlighted in two shades of grey in Fig. 4.

Where multiple samples were taken at different depths within a particular sand unit, it may be possible to ascertain the duration of an arid phase. In some cases, as at Muloorina, deposition was 'geologically instantaneous', with the accumulation of approximately 3 m of sediment around 34.7–32.0 ka, which corresponds to the 34.7–32.0 ka event. At other sites, dune activity was broadly continuous over a long period, such as at Moolawatana between 42 and 27 ka (Fitzsimmons et al., 2007). This suggests two mechanisms of dune accretion—short-lived events and longer-term episodes of activity—consistent with the pattern shown by the age clusters. Individual dunes do not always preserve evidence of all episodes of aeolian reactivation, which is often removed by reworking. The events identified are interpreted to represent brief but regional reactivation of the dunefields. This paper overcomes the limitations of sampling bias in individual dune studies by presenting a chronology using widespread sampling across the dunefields, allowing identification of multiple periods of dune activity.

4.2. Ages of transverse dunes and aeolian material overlying a beach ridge

Several geomorphic features were dated in addition to the linear dunes, placing the linear dune chronology in the context of broader landscape evolution. Four ages were obtained from two small transverse dunes in the southern Strzelecki Desert, underlying the Moolawatana and Brumby III linear dunes and overlying several large transverse palaeoshorelines (Fig. 2C). The age estimates of 105 ± 6 and 110 ± 6 ka at Moolawatana lie within error of each other and suggest short-lived transverse dune activity. The ages at Brumby III of 123 ± 12 and 92.2 ± 11.9 ka may

represent transverse dune formation around the same time (the youngest and oldest ages of each overlap). The transverse dunes overlying the palaeoshorelines formed subsequent to them and are not directly related to lake palaeohydrology; they more likely reflect arid conditions like the linear dunes. Fitzsimmons et al. (2007) demonstrated that transverse dunes at Lake Frome were also active at around the same time as the linear dunes.

At Illusion Plains, a sample was taken from an aeolian unit overlying a beach ridge from which linear dunes, including the Muloorina dune, extend downwind (Fig. 2D). The aim of sampling this feature was to establish whether a chronological relationship existed between the two sites. The aeolian unit at Illusion Plains yielded an age estimate of 190 ± 15 ka, very much older than the Muloorina linear dune downwind, which has a basal age of 87.5 ± 5.3 ka. The difference in age indicates that the current basal linear dune horizon may have formed much later than the Illusion Plains aeolian unit.

4.3. Ages of substrate

Two samples were taken in silty alluvial sand underlying linear dunes at Kelleary and Mudora (Fig. 3). A small ephemeral channel north of the Kelleary site which trends westwards away from the stony tablelands to the east, and several ephemeral channels trending north into the dunefields from a stony hill at Mudora (Fig. 1), may have deposited this material. The two samples of alluvial material yield ages significantly older than the linear dunes, and within error of each other. At Kelleary, a channel was active at 186 ± 10 ka, and channels were active around 193 ± 17 ka at Mudora. The similar ages suggest coeval fluvial activity, and correspond with TL ages of fluvial sands from the Cooper Creek region by Maroulis et al. (2007).

5. Discussion

5.1. Geomorphic implications for the interpretation of dune activity

Linear dune reactivation is primarily a function of sediment supply, and wind strength sufficient for aeolian transport (e.g. McKee, 1979; Wasson and Hyde, 1983). The timing of dune activity therefore reflects the environmental conditions under which sediment becomes available. In desert dunefields, sand can be supplied through two dominant mechanisms. Firstly, climatic change to more arid conditions results in reduced vegetation cover and therefore greater availability of material at the surface. Secondly, sediment may become available through the introduction of material from nearby rivers or lakes, which is also partly a function of climate. Most of the Strzelecki and Tirari dunefields lie beyond the influence of major modern fluvio-lacustrine sediment sources, and therefore dune activity across the region most likely occurred in response to heightened aridity.

The obliquely oriented linear dunes that underlie some parts of the dunefield may be used to infer a change in dune orientation over time in response to changing wind regimes. Since these are not preserved everywhere, most dunes were probably completely reworked over long periods of time. The orientations of the oblique dunes at Hesse and Tirari West (Fig. 2A and B), however, do not correspond to a straightforward latitudinal shift in wind regime as proposed by Sprigg (1982) to account for the continental dune whorl. The two sites provide insufficient evidence to reconstruct changes in the central Australian wind regime over time, but do have implications for the relationship between linear dunes and wind regime. The basal ages of the obliquely oriented dunes are older (66–71 ka) than most linear dunes in the dominant orientation (Fig. 4). However, the younger ages at Hesse indicate dune activity coeval with that in the dominant orientation (Fig. 3). This suggests that obliquely oriented dunes may continue to be active after the change in wind regime as a result of morphological inertia, a term used here to describe the retention of original morphology under conditions which would not necessarily be conducive to perpetuating such forms.

Dune stratigraphy, and its preservation, is crucial to the interpretation of linear dune chronology. As shown in Fig. 3, many of the sites sampled preserve palaeosols between undisturbed sand units, and in some cases, multiple palaeosols were observed. However, it is not possible to constrain the timing of pedogenesis, and therefore periods of hiatus in aeolian activity cannot easily be linked to regional pedogenesis across the dunefields. The propensity for dune reworking and removal of palaeosols further complicates any attempt to correlate individual palaeosols (Fitzsimmons and Telfer, in press).

5.2. Inception of the linear dunefields

It is interesting to observe that no dunes beyond 116 ka, corresponding to Marine Isotope Stage (MIS) 5 in age on the timescale of Martinson et al. (1987), are preserved in this driest part of the Australian continent. This is despite evidence for aridity in Australia originating much earlier (Nanson et al., 1992b; Hesse et al., 2004; Fujioka et al., 2005), and very old ages greater than 600 ka for linear dunes in the Simpson Desert to the northwest (Rhodes et al., 2005). It is almost certain that the Strzelecki and Tirari Desert dunefields existed prior to MIS 5, but that dunes were not preserved from this period due to complete reworking in the last glacial cycle.

There is evidence for aeolian activity in the Strzelecki and Tirari Desert dunefields prior to MIS 5. The 190 ka age of the aeolian unit at Illusion Plains corresponds broadly with the termination of MIS 7 (Fig. 3), coeval with the end of a period of high lake levels at Lake Eyre which resulted in the beach ridge which underlies the unit (Magee, 1998).

The age of this aeolian material presents the possibility that linear dunefields were active in the region at this time, although they have not been preserved in the stratigraphic record. Enhanced aeolian activity involving dust entrainment from the Australian continent during MIS 6 is clearly evident from high mass accumulation rates of dust in the Tasman Sea, and has been linked with dune building (Hesse, 1994).

The alluvial substrate material at Kelleary and Mudora provides evidence for possibly coeval fluvial activity towards the end of MIS 7. Enhanced fluvial activity at this time has been noted elsewhere in central Australia (Nanson et al., 1992b; Maroulis et al., 2007) and corresponds to the high lake levels at Lake Eyre discussed above. The palaeoshoreline immediately east of Lake Frome (Fig. 2C) has also been dated to MIS 7 using *Genyornis* bird eggshell (J. Magee and G. Miller, pers. comm.), and indicates perennial lake conditions causing beach ridge formation. These geomorphic proxies have been linked to wetter conditions which have not occurred since (Nanson et al., 1992b), except during MIS 5 (Magee et al., 2004). The two ages at Kelleary and Mudora indicate that dunefield inception in the vicinity of the alluvial systems postdates MIS 7, but do not preclude the possibility of earlier dune activity elsewhere in the Strzelecki and Tirari Deserts. Given the large errors on these ages and the one at Illusion Plains, it is difficult to discern whether or not aeolian activity was coeval with alluvial transport.

5.3. Linear dunefield activity and palaeoclimatic implications

The linear dune ages group into events around 73–66, 35–32, 22–18, 14–12 and 11.7–10.0 ka. The latter two events, due to their close relationship in time, are discussed as a collective episode between 14 and 10 ka. These discrete groupings appear to reflect widespread episodes of enhanced aeolian activity in the Strzelecki and Tirari dunefields, in response to intensified aridity. The timing of these episodes corresponds to MIS 4, late MIS 3, MIS 2 and the MIS 2-1 transition period respectively, on the timescale of Martinson et al. (1987). The age clusters are significant, since they demonstrate large-scale phases of dune activity, although not all dunes preserve every phase. Ages outside the groups may represent preservation of intermediate partial activity under conditions close to the threshold of aeolian activity, but not sufficiently humid to induce pedogenesis.

The age groupings provide, for the first time, an overview of the timing of enhanced aeolian activity in the central Australian dunefields. The dune record can now be placed in the context of late Quaternary palaeoclimatic change in Australia with some confidence. The peaks in aeolian activity from the Strzelecki and Tirari Desert dune record, shown in Fig. 5, are compared against records of aeolian dust concentration from the Tasman Sea and ice cores in Antarctica (Hesse, 1994; EPICA, 2006), temperature in Antarctica (EPICA, 2006), and the stacked sea surface temperature record from the Australasian region (Barrows et al., 2007). The dust record of Hesse (1994) is shown here on a relative scale, rather than as dust flux, since it is currently under review.

5.3.1. Dune activity prior to MIS 4

The sample site White Dog yielded an age (116 ± 6 ka) significantly older than those from the rest of the dunefield. The site is an isolated linear dune situated on the active floodplain of Cooper Creek, distinct from the main dunefield. The provision of suitably sized fluvial material from Cooper Creek reflects wetter, monsoon-influenced conditions in the headwaters of the catchment further north (Maroulis et al., 2007), and this influx of sediment may have been sufficient to form dunes on the floodplain at this time. The age of White Dog may be linked to an increased availability of sediment coupled with local aridity. Linear and source-bordering dune activity on the floodplain has previously been directly linked to sediment influx from Cooper Creek, particularly around MIS 5 (Nanson et al., 1992b; Maroulis et al., 2007).

The only other sampled instance of dune activity prior to MIS 4 in the Strzelecki and Tirari Deserts occurs at Muloorina near Lake Eyre at 87.5 ± 5.3 ka, during late MIS 5. Dune activity during late MIS 5 is not recorded elsewhere in the dunefield; however, similar ages between 88 and 92 ka were reported for Lake Eyre beach ridges (Magee, 1998; Nanson et al., 1998). Evidence for high lake levels between 130 and 75 ka (Magee et al., 2004) and increased local fluvial activity in the Lake Eyre region (Croke et al., 1999) suggest that conditions were relatively wet, rather than arid, at this time. Linear dune formation at Muloorina may have occurred coevally with beach ridge development rather than in direct response to aridity.

The evidence for pre-MIS 4 linear dune activity is limited to two ages, both of which fall within MIS 5. This is significant; dune activity almost certainly took place prior to this time (e.g. Rhodes et al., 2005), but the current dunefields all postdate the much wetter conditions of MIS 5, during which time sediment was introduced to areas close to lakes and rivers.

5.3.2. Dune activity between 73 and 66 ka

The earliest cluster of ages between 73 and 66 ka coincides with some of the oldest preserved ages for dune activity in both the central Strzelecki Desert (Lomax et al., 2003) and the Simpson Desert to the northwest (Nanson et al., 1998; Hollands et al., 2006). Although Lomax et al. (2003) suggest that the onset of dunefield formation took place around 65 ka, their hypothesis was based on one age estimate overlying alluvial material dated to 69–71 ka; the older dune ages from both this study and others (Rhodes et al., 2005) suggest that dune initiation may have occurred locally around 65 ka, but was not widespread across the Strzelecki and Tirari dunefields.

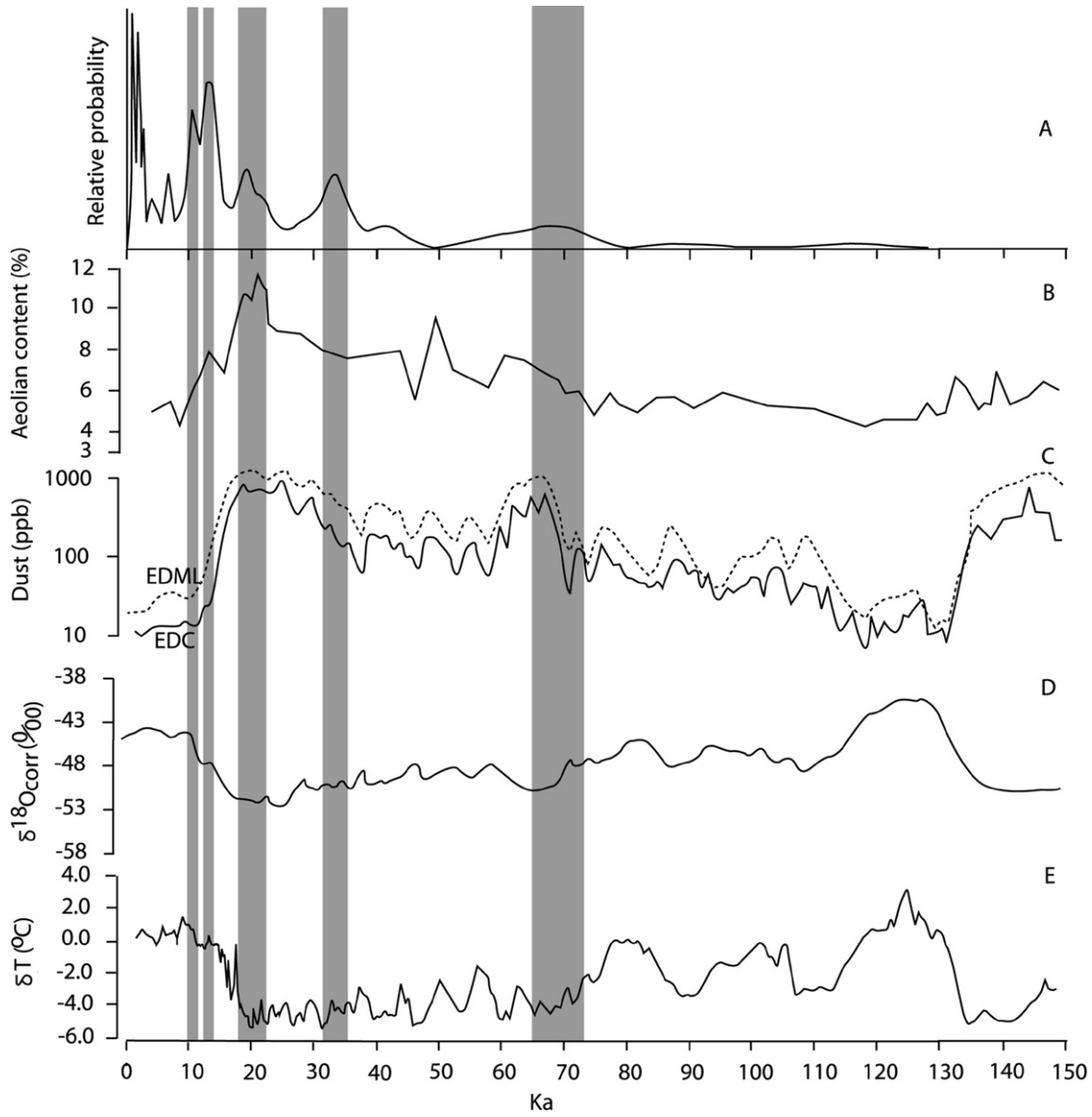

Fig. 5. Comparing the Australian dune record from this study (A) with other palaeoclimatic records; (B) Aeolian concentration of dust in Tasman Sea sediments (Hesse, 1994); (C) dust concentration in the Dronning Maud Land (EDML) and Dome C (EDC) ice cores in Antarctica (EPICA, 2006); (D) $\delta^{18}O$ (corrected) ice volume record from the EDML ice core (EPICA, 2006), and (E) stacked sea-surface temperature record from the Australasian region (Barrows et al., 2007). Age groupings for dune activity are highlighted in grey.

MIS 4 was a time of mixed palaeoclimate signatures across the Australian continent (Hesse et al., 2004). Aridity in the desert dunefields appears to have extended further east, with dry-lake conditions recorded at Lake Mungo in the currently semi-arid Mallee region (Bowler, 1998) and increased dust flux to the Tasman Sea coincident with the intensified aeolian activity (Hesse, 1994; Kawahata, 2002). The expansion of glaciers in the southeast Australian highlands was at its greatest extent around 59 ka, indicating generally colder climates across the continent, with more precipitation than during the LGM but nevertheless relatively dry conditions (Barrows et al., 2001).

During MIS 4, increased dust concentrations coincident with intensified aeolian activity are recorded in the Antarctic ice cores (EPICA, 2006) (Fig. 5), but are not clearly evident in the Tasman Sea sediments (Hesse, 1994), which are assumed to be directly linked to Australian dust flux. The Tasman Sea record registers an increase in dust concentration from approximately 74 ka, peaking around 61 ka (Hesse, 1994). A later dust peak around 52 ka is not reflected in the desert dune record, although this lack of agreement may be a function of low sampling resolution. Sea surface temperature in the Australasian region decreased noticeably from 75 ka (Barrows et al., 2007), and temperature cooled in Antarctica between 70 and 60 ka (EPICA, 2006). Comparison of the dune record with these data suggests that conditions were colder, as well as arid, in the dunefields between approximately 73 and 66 ka.

The episode of aeolian activity between approximately 73 and 66 ka is followed by a conspicuous gap in the dune

record from 58–50 ka. The Hesse, Moolawatana and Muloorina sites all contain palaeosols that must have formed within this period, indicating landscape stability and a hiatus in dune activity. Gypcrete preserved at Lake Eyre around this time also suggests more humid conditions but has not been dated directly (Magee et al., 1995). Beach ridges at Lakes Frome and Eyre were dated using TL to around 60–39 ka (Nanson et al., 1998), although these age estimates included large errors. These data combined clearly suggest that a period of more humid conditions occurred for some time after MIS 4.

5.3.3. Dune activity between 35 and 32 ka

Aridity and enhanced dune activity returned to the dunefields between 35 and 32 ka. This period correlates with dune ages from other studies in the central Strzelecki Desert (Gardner et al., 1987; Lomax et al., 2003), the southern Strzelecki (Wasson, 1983) and Simpson dunefields (Nanson et al., 1992a), and dunes in the Mallee region (Gardner et al., 1987). Hydrologic stress and playa-deflation conditions at Lake Mungo (Bowler et al., 2003) support the evidence for heightened aridity across the interior of the continent at this time. Restricted linear dunes also developed in the currently temperate Blue Mountains around 33 ka, suggesting increased aridity and suppressed vegetation cover close to the east coast of Australia (Hesse et al., 2003). Glaciers readvanced at 32 ka in the Snowy Mountains of Australia, indicating a return of cold conditions (Barrows et al., 2001).

Despite the expansion of linear dunes in response to apparent aridity across the continent, the climate signal from other Australian proxies is more ambiguous. Conditions in the southeast Australian highlands were wetter, or runoff was effectively increased, at this time (Hesse et al., 2004). Increased runoff from the southeast highlands may reflect complex signals from seasonal factors, including increased storage of water in the mountains as snow. Bedload in one of the major eastern Australian rivers, the Murrumbidgee, increased appreciably (Page et al., 1996). The first significant cooling of sea surface temperature occurred in the region and indicates reduced temperatures on the mainland at this time (Barrows et al., 2007).

5.3.4. Dune activity during the LGM and Pleistocene–Holocene transition period

The significant clustering of ages between 22–18 ka, and 14–12 ka and 11.7–10.0 ka (14–10 ka), correspond to the global LGM and Pleistocene–Holocene transition period, respectively. The period around 18–14 ka appears to have been a time of reduced activity, less intense than at 22–18 ka and after 14 ka. Lacustrine sediments indicative of permanent water at Lake Frome were dated by radiocarbon to 18–13 kyr (cal) BP (Draper and Jensen, 1976) during the intervening period, reflecting the reduced aeolian activity.

There is widespread agreement that the Australian desert dunes were active between 22 and 10 ka in the Strzelecki Desert (Bowler and Wasson, 1984; Callen, 1984; Gardner et al., 1987; Lomax et al., 2003), the Simpson Desert (Nanson et al., 1992a; Nanson et al., 1995; Hollands et al., 2006) and northern central Australia (Chen et al., 1995; English et al., 2001). These previous dune chronologies, when compiled together with this dataset, also suggest reduced aeolian activity between 16 and 14 ka. The age clusters identified by this study provide, for the first time, evidence of three distinct events over this period.

The LGM in Australia is considered to have been colder and more arid across the continent (e.g. Hesse et al., 2004). Desert dunes expanded to currently temperate regions of the continent in eastern Australia (Hesse et al., 2003) and Tasmania (Duller and Augustinus, 2006), and dust flux to the Tasman Sea increased (Hesse, 1994). Glaciers in the highland regions of southeast Australia and Tasmania expanded in response to colder conditions, although not as extensively as during MIS 4, most likely due to reduced precipitation in a cold, arid climate (Barrows et al., 2001; Barrows et al., 2002; Mackintosh et al., 2006). Increased flows along the Murrumbidgee River during MIS 2 occurred in response to seasonal snow melt from the highlands rather than increased precipitation, and the increased bedload resulted in the formation of source-bordering dunes (Page et al., 1996). Vegetation responded to colder, drier conditions, from the tropics (Kershaw, 1986) to the southern temperate zone (D'Costa et al., 1989). Elsewhere in the Southern Hemisphere, desert dune activity occurred in response to aridity in southern Africa (Stokes et al., 1998; O'Connor and Thomas, 1999; Thomas and Shaw, 2002) under an intensified wind regime (Stuut et al., 2002). Linear dunes were also active in Brazil (DeOliveira et al., 1999).

The monsoon returned to northern Australia at 14 ka (Wyrwoll and Miller, 2001), resulting in wetter conditions from this time. However, full lake conditions fed by the northern Australian monsoon at Lake Eyre did not develop until 12–10 ka (Magee et al., 2004), and it is likely that the monsoon did not affect regions as far south as the Strzelecki and Tirari Deserts until later, around 10 ka. A protracted reestablishment of monsoon conditions would result in the persistence of arid conditions in central Australia for a longer period of time. This may explain the events between approximately 14 and 10 ka, which occur after a brief hiatus in dune activity, and most likely represent intense arid conditions within the dry core of the continent, prior to the penetration of the monsoon influence on climate there.

Conditions elsewhere, however, were different to those prevailing during the LGM. The deglaciation of the Snowy Mountains around 16 ka (Barrows et al., 2001) suggests that temperature increased across the continent from this time, consistent with sea surface temperature records for the region (Barrows et al., 2007). The result would have been warm, arid conditions around 14–10 ka, similar to those prevailing in the Strzelecki and Tirari dunefields today.

Peaks in dust concentration in the Tasman Sea (Hesse, 1994) and Antarctica (EPICA, 2006) occur during the LGM, but these decrease noticeably after approximately 18 ka (Fig. 5). This supports the hypothesis that dunefields in the driest part of the continent remained active after hemispheric-scale aridity and dust raising declined. Arid conditions contracted from the eastern margins of the continent back to the interior. Furthermore, both Antarctic temperature (EPICA, 2006) and Australasian sea surface temperature (Barrows et al., 2007) increased shortly after the LGM. Enhanced dune activity around 14–12 ka coincides with the timing of the Antarctic Cold Reversal around 13.5–12.5 ka, after which time temperatures continued to rise (Jouzel et al., 1995). Conditions in the Strzelecki and Tirari Deserts may have been warm and arid, with decreased effective precipitation due to rising temperatures.

5.3.5. *Holocene dune activity*

In this study, 16 samples yielded Holocene ages. The early Holocene was marked by a noticeable decrease in dune activity. Broadly continuous dune remobilisation took place from approximately 4 ka to the present. One site (Plinth) yielded an early Holocene age (8.2 ± 0.7 ka); only one other reported site in the Simpson Desert gives comparable ages between 10 and 9 ka (Twidale et al., 2001). Low-level perennial lacustrine conditions at Lake Eyre during the early Holocene suggest a somewhat stronger monsoon, perhaps causing wetter conditions in the region (Magee and Miller, 1998; Magee et al., 2004) which would not have been conducive to extensive dune reactivation within the dunefields.

Several studies show that dune reactivation has occurred during the last 5 kyr, both in the Strzelecki (Gardner et al., 1987; Lomax et al., 2003) and Simpson Deserts (Nanson et al., 1992a; Nanson et al., 1995). This late Holocene activity reflects a change in climate to the warm, arid conditions prevailing in the region currently. An ephemeral playa replaced the lacustrine environments at Lake Eyre from 3 to 4 ka (Magee et al., 2004). The late Holocene drying trend extended to Lake Gregory in northern Australia in response to a weakened monsoon (Wyrwoll and Miller, 2001). It is clear from our dataset that although late Holocene dune activity was widespread, particularly in the northern Tirari Desert (Fig. 3), the dunefields are very much older, and the hypothesis for a Holocene age dunefield (Wopfner and Twidale, 1988) is well and truly disproved.

The palaeoclimatic proxies shown in Fig. 5 show low concentrations of dust and reduced temperature in Antarctica during the late Holocene. The Tasman Sea records do not extend to the late Holocene due to loss of the core top (Hesse, 1994). The Antarctic records, however, suggest subdued aeolian activity and a warmer climate; the latter is consistent with the geomorphic evidence in Australia, where warm, arid conditions appear to have prevailed. Secular cooling of sea surface temperatures occurs from the early Holocene (Barrows et al., 2007), although not to the same extent as during the last glacial period. Overall, dune activity during the late Holocene occurred under warm, arid conditions. Aridity and partial dune activity continues into the present.

6. Conclusions

OSL dating of the Strzelecki and Tirari Deserts indicates distinct periods of enhanced aeolian activity between 73–66, 35–32, 22–18, 14–10 ka. The timing of heightened arid periods responsible for dune reactivation is broadly synchronous with arid conditions occurring elsewhere on the continent (e.g. Hesse et al., 2004; Turney et al., 2006), and in the southern hemisphere (e.g. O'Connor and Thomas, 1999; Thomas and Shaw, 2002), at these times. The warm arid conditions responsible for partial dune activity during the late Pleistocene–Holocene transition period and late Holocene, however, contrast with the cooler, arid glacial periods of major remobilisation during the LGM and earlier.

Interestingly, there is little evidence of dune activity preserved prior to MIS 4. Limited linear dune formation nearby Lake Eyre and Cooper Creek occurred in association with increased sediment availability due to high lake levels (Magee et al., 2004) and sandy fluvial activity (Maroulis et al., 2007) during MIS 5. Although it is almost certain that the dunefields were active earlier than this, no evidence is preserved in the dune stratigraphy. The thickness of stratigraphic horizons deposited during single episodes of aridity relative to dune height (Fig. 3) shows that reworking can be significant, and may completely remove horizons deposited during previous arid periods. The regional-scale sampling strategy employed by this study eliminates bias induced by local reworking to provide a regional overview of the timing of linear dune activity in the Strzelecki and Tirari Deserts of Australia.

Acknowledgements

This research was funded by the Cooperative Research Centre for Landscape Environments and Mineral Exploration (CRC LEME). Thanks to Anna Petts, Martin Young, Fern Beavis, Vic Waclawik, Ian Rayner and Vjeko Matic for assistance in the field, and to Norman Hill for help in the laboratory. Alan Mauger and Vicki Stamoulis of the Department of Primary Industries and Resources of South Australia kindly made available the ASTER satellite image used in Fig. 2A, and John Wilford of Geoscience Australia is thanked for providing the image from the Shuttle DEM in Fig. 2B. Thanks to Lisa Worrall and Colin Pain (Geoscience Australia), Gerald Nanson (University of Wollongong) and an anonymous reviewer for reviewing the manuscript. The authors publish with the permission of the CEO, CRC LEME. CRC LEME is supported by the Australian Government's Cooperative Research Centres Program.

References

Adamiec, G., Aitken, M., 1998. Dose-rate conversion factors: update. Ancient TL 16, 37–50.

Aitken, M.J., 1985. Thermoluminescence Dating. Academic Press, London.

Aitken, M.J., 1998. An Introduction to Optical Dating: the Dating of Quaternary Sediments by the Use of Photon-stimulated Luminescence. Oxford University Press, New York.

Barrows, T.T., Stone, J.O., Fifield, L.K., Creswell, R.G., 2001. Late Pleistocene glaciation of the Kosciuszko Massif, Snowy Mountains, Australia. Quaternary Research 55, 179–189.

Barrows, T.T., Stone, J.O., Fifield, L.K., Creswell, R.G., 2002. The timing of the Last Glacial Maximum in Australia. Quaternary Science Reviews 21, 159–173.

Barrows, T.T., Juggins, S., De Deckker, P., Calvo, E., Pelejero, C., 2007. Long-term sea-surface temperature and climate change in the Australian–New Zealand region. Paleoceanography 22, PA2215, doi:10.1029/2006PA001328.

Bateman, M.D., Frederick, C.D., Jaiswal, M.K., Singhvi, A.K., 2003. Investigations into the potential effects of pedoturbation on luminescence dating. Quaternary Science Reviews 22, 1169–1176.

Bøtter-Jensen, L., 1997. Luminescence techniques: instrumentation and methods. Radiation Measurements 27, 749–768.

Bøtter-Jensen, L., Mejdahl, V., Murray, A.S., 1999. New light on OSL. Quaternary Science Reviews 18, 303–309.

Bøtter-Jensen, L., Bulur, E., Duller, G.A.T., Murray, A.S., 2000. Advances in luminescence instrument systems. Radiation Measurements 32, 523–528.

Bowler, J.M., 1976. Aridity in Australia: age, origins and expression in aeolian landforms and sediments. Earth Science Reviews 12, 279–310.

Bowler, J.M., 1998. Willandra Lakes revisited: environmental framework for human occupation. Archaeology in Oceania 33, 120–155.

Bowler, J.M., Wasson, R.J., 1984. Glacial age environments of inland Australia. In: Vogel, J.C. (Ed.), Late Cainozoic Palaeoclimates of the Southern hemisphere. Balkema, Rotterdam, pp. 183–208.

Bowler, J.M., Johnston, H., Olley, J.M., Prescott, J.R., Roberts, R.G., Shawcross, W., Spooner, N.A., 2003. New ages for human occupation and climatic change at Lake Mungo, Australia. Nature 421, 837–840.

Brookfield, M., 1970. Dune trends and wind regime in central Australia. Zeitschrift fur Geomorphologie N.F. Supplementband 10, 151–153.

Callen, R.A., 1984. Quaternary climatic cycles, Lake Millyera region, southern Strzelecki Desert. Transactions of the Royal Society of South Australia 108, 163–173.

Callen, R.A., Wasson, R.J., Gillespie, R., 1983. Reliability of radiocarbon dating of pedogenic carbonate in the Australian arid zone. Sedimentary Geology 35, 1–14.

Chen, X.Y., Chappell, J., Murray, A.S., 1995. High (ground)water levels and dune development in central Australia: Thermoluminescence dates from gypsum and quartz dunes around Lake Lewis (Napperby), Northern Territory. Geomorphology 11, 311–322.

Croke, J.C., Magee, J.W., Wallensky, E.P., 1999. The role of the Australian Monsoon in the western catchment of Lake Eyre, central Australia, during the Last Interglacial. Quaternary International 57–8, 71–80.

D'Costa, D.M., Edney, P., Kershaw, A.P., DeDeckker, P., 1989. Late Quaternary palaeoecology of Tower Hill, Victoria, Australia. Journal of Biogeography 16, 461–482.

DeOliveira, P., Barreto, A.M.F., Suguio, K., 1999. Late Pleistocene/Holocene climatic and vegetational history of the Brazilian caatinga: the fossil dunes of the middle Sao Francisco River. Palaeogeography, Palaeoclimatology, Palaeoecology 152, 319–337.

Draper, J.J., Jensen, A.R., 1976. The geochemistry of Lake Frome, a playa lake in South Australia. BMR Journal of Australian Geology and Geophysics 1, 83–104.

Duller, G.A.T., Augustinus, P.C., 2006. Reassessment of the record of linear dune activity in Tasmania using optical dating. Quaternary Science Reviews 25, 2608–2618.

English, P., Spooner, N.A., Chappell, J., Questiaux, D.G., Hill, N.G., 2001. Lake Lewis basin, central Australia: environmental evolution and OSL chronology. Quaternary International 83-5, 81–101.

EPICA, 2006. One-to-one coupling of glacial climate variability in Greenland and Antarctica. Nature 444, 195–198.

Fitzsimmons, K.E., in press. Morphological variability in the linear dunefields of the Strzelecki and Tirari Deserts, Australia. Geomorphology, doi:10.1016/j.geomorph.2007.02.004.

Fitzsimmons, K.E., Telfer, M.W., in press. Complexities in the preservation and interpretation of Late Quaternary dune records: examples from the Tirari Desert, Australia and the southwestern Kalahari, South Africa. Chungara (Chilean Journal of Anthropology).

Fitzsimmons, K.E., Bowler, J., Rhodes, E., Magee, J., 2007. Relationships between desert dunes during the late Quaternary in the Lake Frome region, Strzelecki Desert, Australia. Journal of Quaternary Science 22 (5), 549–558.

Fryberger, S.G., 1979. Dune forms and wind regime. In: McKee, E.D. (Ed.), A Study of Global Sand Seas. United States Government Printing Office, Washington, pp. 137–170.

Fujioka, T., Chappell, J., Honda, M., Yatsevich, I., Fifield, K., Fabel, D., 2005. Global cooling initiated stony deserts in central Australia 2–4 Ma, dated by cosmogenic ^{21}Ne–^{10}Be. Geology 33, 993–996.

Gardner, G.J., Mortlock, A.J., Price, D.M., Readhead, M.L., Wasson, R.J., 1987. Thermoluminescence and radiocarbon dating of Australian desert dunes. Australian Journal of Earth Sciences 34, 343–357.

Gentilli, J., 1986. Climate. In: Jeans, D.N. (Ed.), Australia, a Geography: 1. The Natural Environment. Sydney University Press, Sydney, pp. 14–48.

Hesse, P.P., 1994. The record of continental dust from Australia in Tasman Sea sediments. Quaternary Science Reviews 13, 257–272.

Hesse, P.P., Simpson, R.L., 2006. Variable vegetation cover and episodic sand movement on longitudinal desert sand dunes. Geomorphology 81, 276–291.

Hesse, P.P., Humphreys, G.S., Selkirk, P.M., Adamson, D.A., Gore, G.B., Nobes, G.C., Price, D.M., Schwenninger, J.-L., Smith, B., Talau, M., Hemmings, F., 2003. Late Quaternary aeolian dunes on the presently humid Blue Mountains, Eastern Australia. Quaternary International 108, 13–22.

Hesse, P.P., Magee, J.W., van der Kaars, S., 2004. Late Quaternary climates of the Australian arid zone: a review. Quaternary International 118–119, 87–102.

Hollands, C.B., Nanson, G.C., Jones, B.G., Bristow, C.S., Price, D.M., Pietsch, T.J., 2006. Aeolian–fluvial interaction: evidence for Late Quaternary channel change and wind-rift linear dune formation in the northwestern Simpson Desert, Australia. Quaternary Science Reviews 25, 142–162.

Huntley, D.J., Hutton, J.T., Prescott, J.R., 1993. The stranded beach-dune sequence of southeast South Australia: a test of thermoluminescence dating 0–800 ka. Quaternary Science Reviews 12, 1–20.

Jennings, J.N., 1968. A revised map of the desert dunes of Australia. Australian Geographer 10, 408–409.

Jouzel, J., Vaikmae, R., Petit, J.R., Martin, M., Duclos, Y., Stievenard, M., Lorius, C., Toots, M., Melieres, M.A., Burckle, L.H., Barkov, N.I., Kotlyakov, V.M., 1995. The two-step shape and timing of the last deglaciation in Antarctica. Climate Dynamics 11, 151–161.

Kawahata, H., 2002. Shifts in oceanic and atmospheric boundaries in the Tasman Sea (Southwest Pacific) during the late Pleistocene: evidence from organic carbon and lithogenic fluxes. Palaeogeography, Palaeoclimatology, Palaeoecology 184, 225–249.

Kershaw, A.P., 1986. Climatic change and Aboriginal burning in northeast Australia during the last two glacial/interglacial cycles. Nature 322, 47–49.

Lancaster, N., 1981. Palaeoenvironmental implications of fixed dune systems in southern Africa. Palaeogeography, Palaeoclimatology, Palaeoecology 33, 327–346.

Lomax, J., Hilgers, A., Wopfner, H., Grün, R., Twidale, C.R., Radtke, U., 2003. The onset of dune formation in the Strzelecki Desert, South Australia. Quaternary Science Reviews 22, 1067–1076.

Mabbutt, J.A., 1968. Aeolian landforms in central Australia. Australian Geographical Studies 6, 139–150.

Mackintosh, A.N., Barrows, T.T., Colhoun, E.A., Fifield, L.K., 2006. Exposure dating and glacial reconstruction at Mt. Field, Tasmania, Australia, identifies MIS 3 and MIS 2 glacial advances and climatic variability. Journal of Quaternary Science 21, 363–376.

Magee, J.W., 1998. Late Quaternary environments and palaeohydrology of Lake Eyre, arid central Australia. Ph.D. Thesis, Australian National University, Canberra.

Magee, J.W., Miller, G.H., 1998. Lake Eyre palaeohydrology from 60 ka to the present: beach ridges and glacial maximum aridity. Palaeogeography, Palaeoclimatology, Palaeoecology 144, 307–329.

Magee, J.W., Miller, G.H., Spooner, N.A., Questiaux, D., 2004. Continuous 150 k.y. monsoon record from Lake Eyre, Australia: insolation-forcing implications and unexpected Holocene failure. Geology 32, 885–888.

Magee, J.W., Bowler, J.M., Miller, G.H., Williams, D.L.G., 1995. Stratigraphy, sedimentology, chronology and paleohydrology of Quaternary lacustrine deposits at Madigan Gulf, Lake Eyre, South Australia. Palaeogeography, Palaeoclimatology, Palaeoecology 113, 3–42.

Maroulis, J.C., Nanson, G.C., Price, D.M., Pietsch, T., 2007. Aeolian–fluvial interaction and climate change: source-bordering dune development over the past 100 ka on Cooper Creek, central Australia. Quaternary Science Reviews 26, 386–404.

Martinson, D.G., Pisias, N.G., Hays, J.D., Imbrie, J., Moore, T.C., Shackleton, N.J., 1987. Age dating and the orbital theory of the Ice Ages: development of a high resolution 0–300,000-year chronostratigraphy. Quaternary Research 27, 1–29.

McKee, E.D., 1979. Introduction to a study of global sand seas. In: McKee, E.D. (Ed.), A Study of global sand seas. United States Government Printing Office, Washington, pp. 1–20.

Mejdahl, V., 1979. Thermoluminescence dating: beta-dose attenuation in quartz grains. Archaeometry 21, 61–72.

Munyikwa, K., 2005. Synchrony of Southern Hemisphere Late Pleistocene arid episodes: a review of luminescence chronologies from arid aeolian landscapes south of the Equator. Quaternary Science Reviews 24, 2555–2583.

Murray, A.S., Wintle, A.G., 2000. Luminescence dating of quartz using an improved single-aliquot regenerative-dose protocol. Radiation Measurements 32, 57–73.

Murray, A.S., Wintle, A.G., 2003. The single aliquot regenerative dose protocol: potential for improvements in reliability. Radiation Measurements 37, 377–381.

Nanson, G.C., Chen, X.Y., Price, D.M., 1992a. Lateral migration, thermoluminescence chronology and colour variation of longitudinal dunes near Birdsville in the Simpson Desert, central Australia. Earth Surface Processes and Landforms 17, 807–819.

Nanson, G.C., Price, D.M., Short, S.A., 1992b. Wetting and drying of Australia over the past 300 ka. Geology 20, 791–794.

Nanson, G.C., Chen, X.Y., Price, D.M., 1995. Aeolian and fluvial evidence of changing climate and wind patterns during the past 100 ka in the western Simpson Desert, Australia. Palaeogeography, Palaeoclimatology, Palaeoecology 113, 87–102.

Nanson, G.C., Callen, R.A., Price, D.M., 1998. Hydroclimatic interpretation of Quaternary shorelines on South Australian playas. Palaeogeography, Palaeoclimatology, Palaeoecology 144, 281–305.

O'Connor, P.W., Thomas, D.S.G., 1999. The timing and environmental significance of late Quaternary linear dune development in western Zambia. Quaternary Research 52, 44–55.

Olley, J.M., Murray, A., Roberts, R.G., 1996. The effects of disequilibria in the uranium and thorium decay chains on burial dose rates in fluvial sediments. Quaternary Geochronology 15, 751–760.

Page, K.J., Nanson, G.C., Price, D., 1996. Chronology of Murrumbidgee river palaeochannels on the Riverine Plain, southeastern Australia. Journal of Quaternary Science 11, 311–326.

Pell, S.D., Chivas, A.R., Williams, I.S., 2000. The Simpson, Strzelecki and Tirari Deserts: development and sand provenance. Sedimentary Geology 130, 107–130.

Prescott, J.R., Hutton, J.T., 1994. Cosmic ray contributions to dose rates for luminescence and ESR dating: large depths and long term variations. Radiation Measurements 23, 497–500.

Readhead, M.L., 1988. Thermoluminescence dating study of quartz in aeolian sediments from southeast Australia. Quaternary Science Reviews 7, 257–264.

Rhodes, E., Chappell, J., Fujioka, T., Fitzsimmons, K., Magee, J., Aubert, M., Hewitt, D., 2005. The history of aridity in Australia: chronological developments. In: Roach, I.C. (Ed.), Regolith 2005—Ten years of CRC LEME. CRC LEME, Australia.

Rhodes, E.J., 1988. Methodological considerations in the optical dating of quartz. Quaternary Science Reviews 7, 395–400.

Rhodes, E.J., 2007. Quartz single grain OSL sensitivity distributions: implications for multiple grain single aliquot dating. Geochronometria 26, 19–29.

Schwerdtfeger, P., Curran, E., 1996. Climate of the Flinders Ranges. In: Davies, M., Twidale, C.R., Tyler, M.J. (Eds.), Natural History of the Flinders Ranges. Royal Society of South Australia, South Australia, pp. 63–75.

Sprigg, R.C., 1982. Alternating wind cycles of the Quaternary era and their influences on aeolian sedimentation in and around the dune deserts of South Australia. In: Wasson, R.J. (Ed.), Quaternary Dust mantles of China, New Zealand and Australia: Proceedings of a Workshop. Australian National University, Canberra, pp. 211–240.

Stokes, S., Haynes, G., Thomas, D.S.G., Horrocks, J.L., Higginson, M., Malifa, M., 1998. Punctuated aridity in southern Africa during the last glacial cycle—the chronology of linear dune construction in the northeastern Kalahari. Palaeogeography, Palaeoclimatology, Palaeoecology 137, 305–322.

Stuut, J.B.W., Prins, M.A., Schneider, R.R., Weltje, G.J., Jansen, J.H.F., Postma, G., 2002. A 300 kyr record of aridity and wind strength in southwestern Africa: inferences from grain-size distributions of sediments on Walvis Ridge, SE Atlantic. Marine Geology 180, 221–223.

Thomas, D.S.G., Shaw, P.A., 2002. Late Quaternary environmental change in central southern Africa: new data, synthesis, issues and prospects. Quaternary Science Reviews 21, 783–797.

Thomas, D.S.G., O'Connor, P.W., Bateman, M.D., Shaw, P.A., Stokes, S., Nash, D.J., 2000. Dune activity as a record of late Quaternary aridity in the northern Kalahari: new evidence from northern Namibia interpreted in the context of regional arid and humid chronologies. Palaeogeography, Palaeoclimatology, Palaeoecology 156, 243–259.

Tsoar, H., Blumberg, D.G., Stoler, Y., 2004. Elongation and migration of sand dunes. Geomorphology 57, 293–302.

Turney, C.S.M., Haberle, S., Fink, D., Kershaw, A.P., Barbetti, M., Barrows, T.T., Black, M., Cohen, T.J., Correge, T., Hesse, P.P., Hua, Q., Johnston, R., Morgan, V., Moss, P., Nanson, G., VanOmmen, T., Rule, S., Williams, N.J., Zhao, J.X., D'Costa, D., Feng, Y.X., Gagan, M., Mooney, S., Xia, Q., 2006. Integration of ice-core, marine and terrestrial records for the Australian Last Glacial Maximum and Termination: a contribution from the OZ INTIMATE group. Journal of Quaternary Science 21, 751–761.

Twidale, C.R., 1972. Evolution of sand dunes in the Simpson Desert, central Australia. Transactions of the Institute of British Geographers 56, 77–109.

Twidale, C.R., Prescott, J.R., Bourne, J.A., Williams, F.M., 2001. Age of desert dunes near Birdsville, southwest Queensland. Quaternary Science Reviews 20, 1355–1364.

Wasson, R.J., 1983. The Cainozoic history of the Strzelecki and Simpson dunefields (Australia), and the origin of desert dunes. Zeitschrift fur Geomorphologie Supplementband 45, 85–115.

Wasson, R.J., Fitchett, K., Mackey, B., Hyde, R., 1988. Large-scale patterns of dune type, spacing and orientation in the Australian continental dunefield. Australian Geographer 19, 89–104.

Wasson, R.J., Hyde, R., 1983. Factors determining desert dune type. Nature 304, 337–339.

Wopfner, H., Twidale, C.R., 1988. Formation and age of desert dunes in the Lake Eyre depocentres in central Australia. Geologische Rundschau 77, 815–835.

Wyrwoll, K.H., Miller, G.H., 2001. Initiation of the Australian summer monsoon 14,000 years ago. Quaternary International 83–85, 119–128.